








Defective cyclophilin A induces TDP-43 proteinopathy: implications for amyotrophic lateral sclerosis and frontotemporal dementia

Laura Pasetto,¹ Maurizio Grassano,² Silvia Pozzi,³ Silvia Luotti,¹ Eliana Sammali,¹ Alice Migazzi,⁴  Manuela Basso,^{1,4} Giovanni Spagnoli,^{4,5} Emiliano Biasini,^{4,5} Edoardo Micotti,¹ Milica Cerovic,¹ Mirjana Carli,¹  Gianluigi Forloni,¹  Giovanni De Marco,² Umberto Manera,² Cristina Moglia,² Gabriele Mora,⁶ Bryan J. Traynor,^{7,8,9} Adriano Chiò,²  Andrea Calvo² and  Valentina Bonetto¹

Aggregation and cytoplasmic mislocalization of TDP-43 are pathological hallmarks of amyotrophic lateral sclerosis and frontotemporal dementia spectrum. However, the molecular mechanism by which TDP-43 aggregates form and cause neurodegeneration remains poorly understood. Cyclophilin A, also known as peptidyl-prolyl cis-trans isomerase A (PPIA), is a foldase and molecular chaperone. We previously found that PPIA interacts with TDP-43 and governs some of its functions, and its deficiency accelerates disease in a mouse model of amyotrophic lateral sclerosis.

Here we characterized PPIA knock-out mice throughout their lifespan and found that they develop a neurodegenerative disease with key behavioural features of frontotemporal dementia, marked TDP-43 pathology and late-onset motor dysfunction.

In the mouse brain, deficient PPIA induces mislocalization and aggregation of the GTP-binding nuclear protein Ran, a PPIA interactor and a master regulator of nucleocytoplasmic transport, also for TDP-43. Moreover, in absence of PPIA, TDP-43 autoregulation is perturbed and TDP-43 and proteins involved in synaptic function are downregulated, leading to impairment of synaptic plasticity. Finally, we found that PPIA was downregulated in several patients with amyotrophic lateral sclerosis and amyotrophic lateral sclerosis-frontotemporal dementia, and identified a PPIA loss-of-function mutation in a patient with sporadic amyotrophic lateral sclerosis. The mutant PPIA has low stability, altered structure and impaired interaction with TDP-43.

These findings strongly implicate that defective PPIA function causes TDP-43 mislocalization and dysfunction and should be considered in future therapeutic approaches.

1 Istituto di Ricerche Farmacologiche Mario Negri IRCCS, 20156 Milano, Italy

2 'Rita Levi Montalcini' Department of Neuroscience, University of Torino, Torino, Italy

3 CERVO Brain Research Centre, Québec City, Québec, Canada

4 Department of Cellular, Computational and Integrative Biology (CIBIO), University of Trento, Trento, Italy

5 Dulbecco Telethon Institute, University of Trento, Trento, Italy

- 6 Department of Neurorehabilitation, ICS Maugeri IRCCS, Milano, Italy
7 Neuromuscular Diseases Research Section, Laboratory of Neurogenetics, National Institute on Aging, NIH, Bethesda, MD 20892, USA
8 Department of Neurology, Johns Hopkins University Medical Center, Baltimore, MD 21287, USA
9 Reta Lila Weston Institute, UCL Queen Square Institute of Neurology, University College London, London, UK

Correspondence to: Valentina Bonetto
Department of Biochemistry and Molecular Pharmacology
Istituto di Ricerche Farmacologiche Mario Negri IRCCS
Via Mario Negri 2, 20156 Milano, Italy
E-mail: valentina.bonetto@marionegri.it

Keywords: TDP-43 pathology; mouse model; nucleocytoplasmic transport; Ran; FTD; ALS

Abbreviations: ALS = amyotrophic lateral sclerosis; e/iPPIA = extracellular/intracellular PPIA; FTD = frontotemporal dementia; PBMC = peripheral blood mononuclear cell; Ran = GTP-binding nuclear protein Ran; TDP-43 = TAR DNA-binding protein-43

Introduction

TAR DNA-binding protein-43 (TDP-43), encoded by the TARDBP gene, is a predominantly nuclear RNA/DNA-binding protein that exerts vital functions in various steps of RNA metabolism, shuttling between the nucleus and the cytoplasm.¹ To do that, TDP-43 physiological levels and correct localization have to also be tightly controlled through autoregulation.^{2,3}

Cytoplasmic mislocalization of TDP-43 and aggregation of its hyperphosphorylated, ubiquitinated and C-terminal fragmented forms are common histopathological hallmarks of the amyotrophic lateral sclerosis (ALS) and frontotemporal dementia (FTD) disease spectrum.^{4,5} TDP-43 proteinopathy is observed in ~97% of ALS and ~50% of FTD patients, in brain and spinal cord, but also in peripheral blood mononuclear cells (PBMCs).^{6,7} TARDBP mutations in ALS and FTD cases have established a direct link between TDP-43 abnormalities and neurodegeneration. However, the molecular mechanism by which TDP-43 aggregates form and cause neurodegeneration remains poorly understood. Besides impairments in RNA and protein homeostasis, nucleocytoplasmic transport defects are emerging as converging disease mechanisms in ALS/FTD.^{8,9} Therapeutic interventions aiming to target the triad of TDP-43 control, i.e. autoregulation, nucleocytoplasmic transport and aggregation, is viewed as a promising strategy to prevent neurodegeneration.¹⁰

Cyclophilin A/peptidyl-prolyl cis-trans isomerase A (PPIA) is highly expressed in the CNS, where it localizes mainly in neurons.¹¹ Despite its abundance, its primary function in the CNS remains largely undefined. PPIA is involved in several cellular processes with double-edged functions. Inside the cells it is mainly beneficial. Besides promoting *de novo* protein folding,¹² it acts as a molecular chaperone and protects against oxidative stress and protein misfolding.^{13–15} PPIA interacts with heterogeneous nuclear ribonucleoproteins (hnRNPs), regulates their nucleocytoplasmic transport and plays a role in the stability of the RNP complexes.^{13,16} PPIA interacts with TDP-43 and governs some of its functions.¹³ In particular, it influences TDP-43 binding to its RNA targets affecting the expression of genes, such as HDAC6, ATG7, VCP, FUS and GRN, involved in the clearance of protein aggregates, and/or mutated in ALS and FTD.¹³ Since PPIA Lys-acetylation favours the interaction with TDP-43, a post-translational regulation is hypothesized. Extracellularly, PPIA behaves as a proinflammatory cytokine.¹⁷ Aberrantly secreted in response to stress, PPIA

activates an EMMPRIN/CD147-NF- κ B-MMP-9 pathway, promoting neuroinflammation and selective motor neuron death.¹⁸

Although PPIA has been studied in connection with several human diseases, some neurodegenerative, its role in pathogenesis has not been established.¹⁹ We first reported that PPIA is altered in ALS.^{20–22} In particular, we observed that PPIA accumulates in Triton-insoluble protein aggregates from the spinal cord in ALS mouse models and sporadic patients.²⁰ Next, we reported that low levels of soluble PPIA in PBMCs of ALS patients are associated with early onset of the disease²³ and short disease duration.⁷ In agreement with this, PPIA deficiency exacerbated aggregation and accelerated disease progression in a mutant SOD1 mouse model of ALS.¹³ However, selective inhibition of extracellular PPIA protected motor neurons, reduced neuroinflammation and increased survival.¹⁸

In previous work, we noted that PPIA knock-out (PPIA^{–/–}) mice presented features of TDP-43 pathology but with no overt clinical phenotype up to 4 months of age.¹³ Here we have characterized PPIA^{–/–} mice neuropathologically and behaviourally throughout their entire lifespan and found that they develop a neurodegenerative disease with marked TDP-43 pathology. PPIA is also defective in several sporadic ALS and ALS-FTD patients, and a rare loss-of-function PPIA mutation was identified in an ALS patient, supporting its involvement in the aetiopathogenesis.

Materials and methods

Animal model

Procedures involving animals and their care were conducted in conformity with the following laws, regulations, and policies governing the care and use of laboratory animals: Italian Governing Law (D.lgs 26/2014; Authorization 19/2008-A issued 6 March, 2008 by Ministry of Health); Mario Negri Institutional Regulations and Policies providing internal authorization for persons conducting animal experiments (Quality Management System Certificate, UNIENISO9001:2008, Reg. No. 6121); the National Institutes of Health's Guide for the Care and Use of Laboratory Animals (2011 edition), and European Union directives and guidelines (EEC Council Directive, 2010/63/UE). The Mario Negri Institutional Animal Care and Use Committee and the Italian Ministry of Health (Direzione Generale della Sanità Animale e dei Farmaci Veterinari, Ufficio 6) prospectively reviewed and approved the animal

research protocols of this study (protocol no. 14–02/C and 9F5F5.60) and ensured compliance with international and local animal welfare standards.

PPIA^{−/−} mice were originally generated and characterized as described.^{24,25} We obtained PPIA^{−/−} mice (strain 129S6/SvEvTac Ppiatm1Lubn/Ppiatm1Lbn; stock no. 005320) from the Jackson Laboratory; they were maintained on a 129S6/SvEvTac background. The PPIA^{−/−} mice on 129S6/Sv genetic background and corresponding PPIA^{+/+} littermates were used for micro-CT, MRI, immunohistochemistry, biochemistry, long-term potentiation, rotarod, grid test and extension reflex, and are hereafter referred to as PPIA^{−/−} mice. PPIA^{−/−} mice on C57BL/6J genetic background (C57_PPIA^{−/−} mice), kindly provided by Dr Bradford C. Berk (University of Rochester Medical Center, Rochester, NY, USA), and corresponding PPIA^{+/+} littermates, were used for cognitive tests (open field, elevated-plus maze, three-chamber sociability, Morris water maze, and novel object recognition). Animals were bred and maintained at the Istituto di Ricerche Farmacologiche Mario Negri IRCCS, Milano, Italy, as described in the [Supplementary material](#).

Micro-CT and MRI

Micro-CT and MRI analysis were done essentially as previously described.^{26,27} Further details are reported in the [Supplementary material](#).

Immunohistochemistry

Immunohistochemistry was done on coronal sections of brain for TDP-43, phosphorylated TDP-43 (pTDP-43), glial fibrillary acidic protein (GFAP), Iba-1, and GTP-binding nuclear protein Ran (Ran) as described in the [Supplementary material](#). Nissl staining was done on brain and lumbar spinal cord sections, as described in the [Supplementary material](#).

Neurofilament light chain measurements

Plasma samples were collected from PPIA^{+/+} and PPIA^{−/−} mice in K2-EDTA BD Microtainer blood collection tube and centrifuged at 5000g for 5 min to isolate plasma sample. Plasma neurofilament light chain (NFL) concentration was measured using the Simoa[®] NF-light[™] Advantage (SR-X) Kit (no. 103400) on the Quanterix SR-X[™] platform with reagents from a single lot, according to the protocol issued by the manufacturer (Quanterix Corp).

Subcellular fractionation

Nuclear and cytoplasmic fractions were isolated from mouse cortex and cerebellum essentially as described.^{13,18} Further details are reported in the [Supplementary material](#).

Extraction of detergent-insoluble proteins

Mouse tissues were homogenized and the Triton-insoluble fraction was obtained essentially as described by Lauranzano et al.¹³ Quantification of the insoluble and soluble protein fractions was done as described in the [Supplementary material](#).

Immunoblotting

Western blot and dot blot were done as previously described.^{7,20} The antibodies used for immunoblot are reported in the [Supplementary material](#).

Real-time PCR

The total RNA from mouse cortex and human PBMC was extracted using the RNeasy[®] Mini Kit (Qiagen) and real-time PCR was done as described in the [Supplementary material](#).

Long-term potentiation analysis

Coronal brain slices (350 µm) were cut and processed for long-term potentiation (LTP) recordings as described in the [Supplementary material](#).

Behavioural analysis

In this study, both male and female mice were tested, at 6 and 12 months of age. All behavioural tests were done at the same time of day, in the afternoon. Mice were allowed to habituate to the test room for at least 1 h. Test environments were thoroughly cleaned between test sessions and males were tested before females. The open field, elevated-plus maze, three-chamber sociability, Morris water maze and novel object recognition test used Ethovision XT, 5.0 software (Noldus Information Technology, Wageningen, The Netherlands) to record the parameters. Further details are described in the [Supplementary material](#).

Muscle atrophy

Tibialis anterior muscles were freshly dissected, as previously described,²⁸ immediately frozen and weighted on an analytical balance with 0.1 mg readability and 0.2 mg linearity (Crystal series, Gibertini). To evaluate muscle atrophy, the weight of the muscle was normalized to mouse body weight.

Participants in the study

Informed written consent was obtained from all participants involved and the study was approved by the ethics committee of Azienda Ospedaliero Universitaria Città della Salute e della Scienza, Turin and ICS Maugeri IRCCS, Milano. The diagnosis of ALS was based on a detailed medical history and physical examination, and confirmed by electrophysiological evaluation. Inclusion criteria for ALS patients were: (i) 18–85 years old; and (ii) had a diagnosis of definite, probable or laboratory-supported probable ALS, according to revised El Escorial criteria.²⁹ Exclusion criteria were: (i) diabetes or severe inflammatory conditions; (ii) active malignancy; and (iii) pregnancy or breast-feeding. ALS patients underwent a battery of neuropsychological tests and were classified according to the consensus criteria for the diagnosis of frontotemporal cognitive and behavioural syndromes in ALS.^{30–32} We analysed clinical samples from three independent cohorts of ALS patients and control participants (Cohorts 1–3), totalling 151 ALS patients and 128 healthy participants. The characteristics of the patients and controls are described in [Supplementary Table 1](#).

Isolation of peripheral blood mononuclear cells and plasma

Blood was drawn by standard venipuncture into Vacutainer[®] Plus Plastic K2EDTA Tubes (Becton, Dickinson and Company) and kept at 4°C until shipment to the Istituto di Ricerche Farmacologiche Mario Negri IRCCS. PBMCs were isolated from ALS patients and healthy individuals, as previously described.⁷ Further details are described in the [Supplementary material](#).

Mutation screening

We examined a cohort of 959 ALS patients from Northern Italy and 677 healthy controls matched by age, sex and geographical origin. Informed written consent was obtained for all participants, and the study was approved by the ethics committees involved. Whole-genome sequencing was done at The American Genome Center (Uniformed Services University, Walter Reed National Military Medical Center campus, Bethesda, MD, USA) as described in the [Supplementary material](#).

Molecular dynamics simulations

The structure of wild-type PPIA was retrieved from PDB 1CWA. The mutant form was generated by swapping the lysine 76 with glutamate using UCSF Chimera.³³ Molecular dynamics simulations were carried out as described in the [Supplementary material](#).

Comparative analysis with retrospective cohort

To compare protein levels of the PPIA K76E patient with the retrospective cohort analysed in Luotti *et al.*⁷ PBMCs were isolated and proteins extracted exactly as previously reported.⁷ Slot blot analysis was done with the same internal standard as the previous work, which is a pool of all samples in the analysis. Immunoreactivity was normalized to Red Ponceau staining (Fluka) and to the immunosignal of the internal standard.

AlphaLISA assay of MMP-9

The level of MMP-9 in plasma was measured with an AlphaLISA kit for the human protein (no. AL3138, PerkinElmer). AlphaLISA signals were measured using an Ensign Multimode Plate Reader (PerkinElmer).

Cell and molecular biology procedures

Mutant PPIA cloning, cell culture, transfection and treatments were done as described in the [Supplementary material](#).

Immunoprecipitation

Magnetic beads coupled with sheep polyclonal antibodies anti-rabbit IgG (Dynabeads, Invitrogen) were used for co-immunoprecipitation studies. Cells were lysed in 50 mM Tris-HCl, pH 7.2, 2% CHAPS, protease inhibitor cocktail (Roche) and quantified with the BCA protein assay (Pierce). Proteins (500 µg) were diluted to 0.5 µg/µl with lysis buffer. Magnetic beads with coupled sheep antibodies anti-rabbit IgG (Dynabeads® M280; Invitrogen) were washed with 0.5% bovine serum albumin immunoglobulin-free (BSA Ig-free) in PBS to remove preservatives. Then 3 µg of rabbit polyclonal antihuman TDP-43 primary antibody (Proteintech; RRID: AB_2200505) or rabbit polyclonal antihuman Ran primary antibody (Abcam) was incubated with 20 µl of anti-rabbit IgG-conjugated Dynabeads for 2 h at 4°C in 0.1% BSA/PBS. Immunoprecipitation and analysis of the proteins are described in the [Supplementary material](#).

Statistical analysis

Prism 7.0 (GraphPad Software Inc., San Diego, CA) was used. For each variable, the differences between experimental groups were analysed by Student's *t*-test, or one-way ANOVA followed by post hoc tests. Pearson's correlation coefficient (*r*) was calculated to measure the linear strength of the association between PPIA and TDP-43 total protein levels. Two-way ANOVA followed by the Bonferroni post hoc test was used to analyse rotarod, grid,

extension reflex and body weight of PPIA^{−/−} mice and controls. Survival curves were analysed using a log-rank Mantel–Cox test. *P*-values below 0.05 were considered significant.

Data availability

The whole-genome sequence data is publicly available on dbGaP at phs001963. The other data that support the findings of this study are available within the paper and [Supplementary material](#). Raw data have been deposited in the Zenodo public repository (<https://doi.org/10.5281/zenodo.5730038>).

Results

PPIA is defective in patients with sporadic ALS

In PBMCs of ALS patients we detected a low level of Lys-acetylated PPIA.¹³ We also observed, an impaired soluble/insoluble partitioning of PPIA and TDP-43 in PBMCs of a relatively large cohort of sporadic ALS and ALS-FTD patients in comparison with healthy control participants, with significant accumulation of PPIA and TDP-43 in the insoluble fraction and substantially less PPIA in the soluble fraction.⁷ Here we measured the total PPIA and TDP-43 protein levels in the retrospective cohort (Cohort 1, [Supplementary Table 1](#)). PPIA was significantly lower than controls, while TDP-43 did not differ ([Fig. 1A and B](#)). We checked whether this reflected downregulation of the PPIA gene. There was in fact significant downregulation of PPIA at the mRNA level too, in an independent cohort of sporadic ALS patients compared to healthy controls (Cohort 2, [Supplementary Table 1](#)), and only a tendency to lower TARDBP mRNA ([Fig. 1C and D](#)). Finally, we detected a significant, although weak, positive correlation (*r* = 0.3, *P* = 0.01) between PPIA and TDP-43 total protein levels.

In conclusion, defective PPIA is a common feature of ALS and ALS-FTD patients and could trigger TDP-43 pathology.

PPIA^{−/−} mice display neuropathological alterations, worsening with age

To explore PPIA's impact on TDP-43 biology we did deep characterization of PPIA^{−/−} mice throughout their lifespan. In our previous studies PPIA^{−/−} mice had a higher burden of Triton-insoluble phosphorylated TDP-43 (insoluble pTDP-43) in the spinal cord and brain cortex already at 4 months of age.¹³ We detected no motor neuron loss¹⁸ and no motor phenotype ([Supplementary Fig. 1A and B](#)), but there was a tendency to kyphosis ([Supplementary Fig. 1C](#)).

To see whether these were prodromal signs of neurodegeneration, we carried out a neuropathological analysis of older PPIA^{−/−} mice. Quantitative MRI was done longitudinally on PPIA^{−/−} and PPIA^{+/+} mice at 6 and 12 months. PPIA^{−/−} mice had a smaller total brain volume than controls, with the most marked difference at 12 months (−13%) ([Supplementary Fig. 1D](#)).

Next, we verified the effect of PPIA depletion on hippocampus, cortex and cerebellum, adjusting for total brain volume ([Fig. 2](#) and [Supplementary Fig. 1](#)). PPIA^{−/−} mice had a significantly smaller hippocampus than PPIA^{+/+} mice at 6 and 12 months ([Fig. 2A](#)). There was also a reduction of the relative volume with age, independently from the genotype, slightly more marked in PPIA^{−/−} mice (−23% versus −21%). The cortex volume of PPIA^{−/−} mice was also smaller than in PPIA^{+/+} mice, but less so (3% and 10% smaller at 6 and 12 months of age, respectively), and the difference was significant only at 12 months ([Fig. 2B](#)). However, PPIA^{−/−} mice had significant cortex atrophy at 12 compared to 6 months (−16%); this was less marked in control mice (−10%). In contrast, cerebellum relative volume did not significantly differ

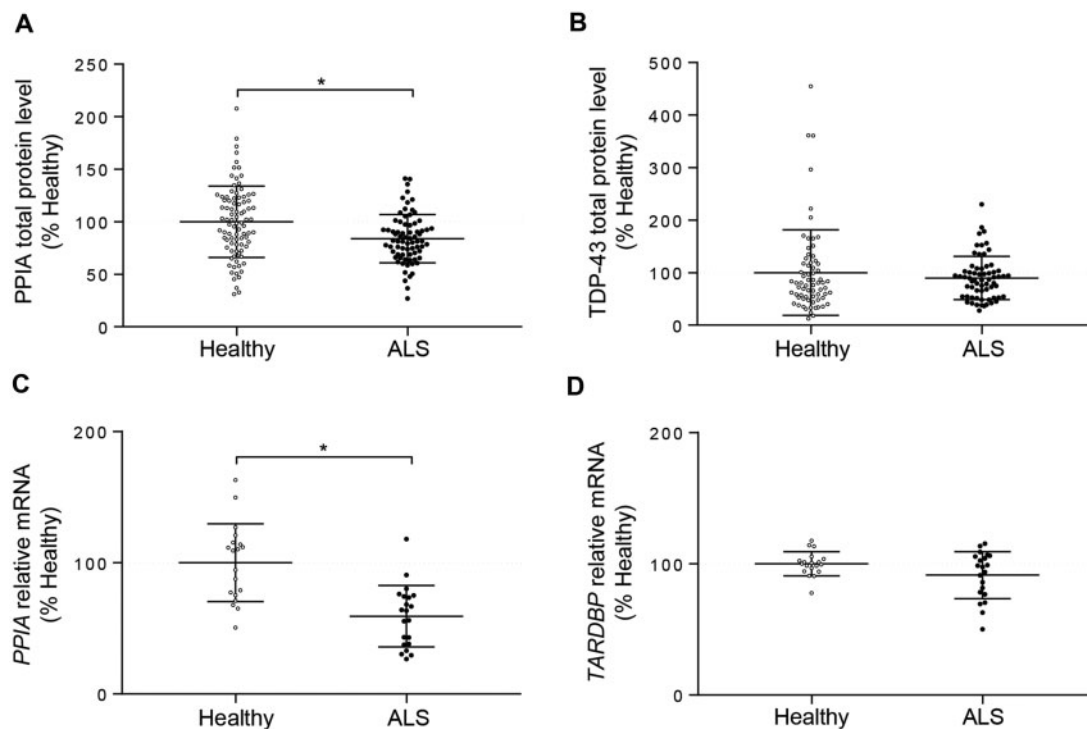


Figure 1 PPIA is downregulated in sporadic ALS patients. (A and B) Total PPIA (A) and TDP-43 (AB_2200505) (B) protein levels were analysed in PBMCs from ALS patients and healthy participants of a retrospective cohort⁷ (Cohort 1, [Supplementary Table 1](#)). Scatter dot plots (mean \pm SD; PPIA: $n = 89$ healthy controls, $n = 74$ ALS patients; TDP-43: $n = 69$ healthy controls, $n = 65$ ALS patients) are percentages of healthy controls and the dotted lines indicate the median of healthy controls; * $P < 0.05$ versus healthy controls, Student's t -test. (C and D) Real-time PCR for PPIA (C) and TARDBP (D) mRNA transcripts in PBMCs of ALS patients and healthy participants (Cohort 2, [Supplementary Table 1](#)). Data (mean \pm SD; $n = 19$ healthy participants; $n = 21$ ALS patients) are normalized to β -actin and expressed as percentages of the healthy control relative mRNA. Dotted lines indicate the median of healthy controls; * $P < 0.05$ versus healthy controls, Student's t -test.

in PPIA $^{-/-}$ mice and controls and did not change with age ([Supplementary Fig. 1E](#)).

To investigate whether brain atrophy reflected neuronal loss we did a histological analysis on the hippocampus and cortex ([Fig. 2C and D](#)). There were substantially fewer Nissl-positive neurons in the hippocampus CA1 region of PPIA $^{-/-}$ mice than in controls at 6 and 12 months, and this tended to be more pronounced at 12 months ([Fig. 2C](#)). In the cortex PPIA $^{-/-}$ mice had fewer Nissl-positive neurons than controls at 6 and 12 months, but this was significant only at 12 months ([Fig. 2D](#)). They also had significantly greater neuron loss at 12 months than at 6 months, similarly to the MRI picture. The progressive neurodegenerative process in PPIA $^{-/-}$ mice was also confirmed by the plasma NFL level, a marker of neuro-axonal damage, which increased substantially with age compared to controls from 6 months ([Fig. 2E](#)).

We next examined the glial response in the hippocampus and cortex of PPIA $^{-/-}$ mice ([Fig. 2F](#) and [Supplementary Fig. 1F and G](#)). In the hippocampus, PPIA deficiency tended to increase astroglial activation at 12 months ([Fig. 2F](#)), but had no effect on microglia ([Supplementary Fig. 1F](#)). In the cortex, PPIA deficiency did not affect either astroglia or microglia ([Supplementary Fig. 1G](#)), confirming PPIA role in microglial activation and the neuroinflammatory response.¹⁸

To explore whether the neuropathological alterations were associated with TDP-43 pathology, we did biochemical and immunohistochemistry analyses for TDP-43 and pTDP-43 in brains of PPIA $^{-/-}$ mice and controls at 6 and 12 months of age ([Fig. 3](#) and [Supplementary Fig. 2](#)). In the cortex of PPIA $^{-/-}$ mice there was a significant increase in pTDP-43 in the cytoplasm and a concomitant decrease of TDP-43 in the nucleus compared to controls

already at 6 months ([Fig. 3A](#)), while we saw no change in cerebellum ([Supplementary Fig. 2A](#)). We analysed the Triton-insoluble protein fraction from brain cortex of PPIA $^{-/-}$ and PPIA $^{+/+}$ mice and found that in PPIA $^{-/-}$ mice there was significantly larger number of insoluble proteins, TDP-43 and pTDP-43 ([Supplementary Fig. 2B–D](#)). We also analysed other proteins associated with ALS/FTD that interact with TDP-43 in RNP complexes and/or stress granules ([Supplementary Fig. 2E and F](#)). In the absence of PPIA, there was a higher level of insoluble hnRNPA2/B1 and TIA1, confirming the negative effect of deficient PPIA folding/refolding activity in the brain.¹³

Finally, we examined TDP-43 fragmentation in soluble and insoluble brain cortex fractions ([Fig. 3B](#)). Characteristic C-terminal 35- and 25-kDa TDP-43 fragments were abundant, mainly in the insoluble fraction. While TDP-43 bands at 43 and 35 kDa, respectively, slightly decrease (–6%) and increase (+12%) in PPIA $^{-/-}$ mice, but not significantly (data not shown), the 25-kDa TDP-43 fragment accumulated substantially (+61%). As often happens in patients with ALS/FTD,^{34,35} the burden of TDP-43 C-terminal fragments is greater than that of full-length TDP-43 and the 25 kDa accumulates more than the 35 kDa fragment, probably because it is less readily degraded.³⁶

To explore TDP-43 pathology and C-terminal TDP-43 fragments, we did a histopathological analysis with an antibody that targets the C-terminus of the protein.³⁷ At 12 months of age, there was a widespread TDP-43 signal in different brain regions of PPIA $^{-/-}$ mice, with higher intensity in hippocampus and cortex, that accumulates in aggregated structures ([Fig. 3C–E](#)). We confirmed the presence of TDP-43 inclusions in PPIA $^{-/-}$ brain regions using a pTDP-43 antibody that targets the C-terminus, does not

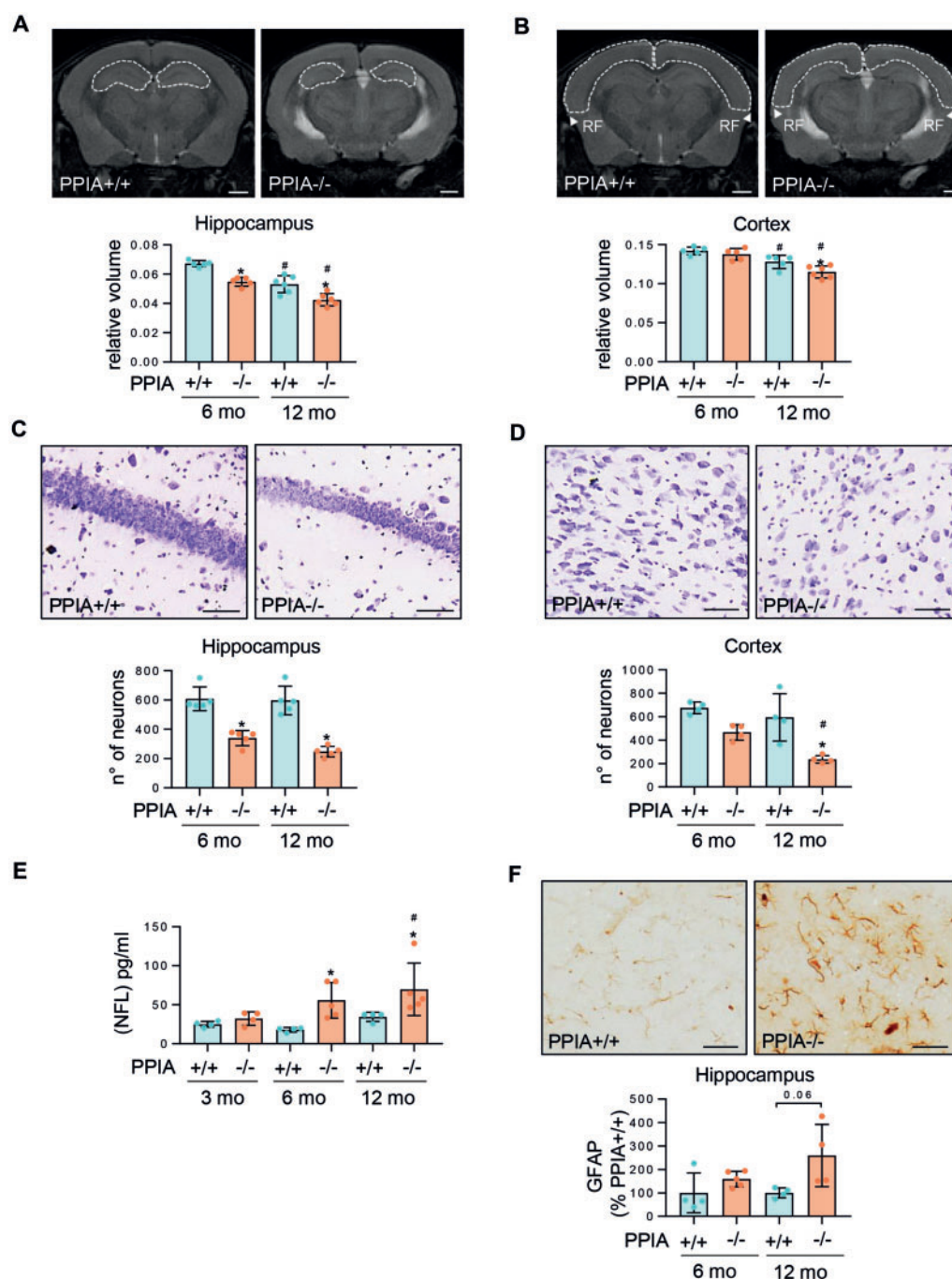


Figure 2 PPIA^{-/-} mice show progressive neuropathological alterations. (A and B) The volume of hippocampus (A) and cortex (B) was measured using quantitative MRI in PPIA^{+/+} and PPIA^{-/-} mice, at 6 and 12 months (mo) of age. Representative MRI images of PPIA^{+/+} and PPIA^{-/-} brain regions at 12 months are shown. The white dashed lines indicate the region of interest considered for MRI quantification. Scale bar = 1 mm. The volume of hippocampus and cortex were adjusted for total brain volume and data are expressed as relative volume, mean \pm SD ($n = 5$ or 6 in each experimental group). (C and D) Depletion of PPIA induces progressive neuron loss. Neurons in CA1 region (C) and cortex (D) were counted in PPIA^{+/+} and PPIA^{-/-} mice at 6 and 12 months. Representative Nissl-stained brain section are shown. Scale bar = $50 \mu\text{m}$. Mean \pm SD ($n = 5$, CA1 region; $n = 4$, cortex). (E) NFL plasma levels were analysed in PPIA^{+/+} and PPIA^{-/-} mice at 3, 6 and 12 months. Data are mean \pm SD ($n = 4$ or 5 in each experimental group); * $P < 0.05$ versus PPIA^{+/+} mice and * $P < 0.05$ versus the 3 months, by one-way ANOVA, uncorrected Fisher's least significant difference (LSD) post hoc test. (F) GFAP-immunostaining in hippocampus was quantified in PPIA^{+/+} and PPIA^{-/-} mice at 6 and 12 months. Representative GFAP-stained brain sections are shown. Scale bar = $50 \mu\text{m}$. Data (mean \pm SD; $n = 4$ or 5 in each experimental group) are percentages of the PPIA^{+/+}; (A–D and F) * $P < 0.05$ versus the PPIA^{+/+} mice and * $P \leq 0.05$ versus the 6 months, by one-way ANOVA, Tukey's post hoc test.

react with physiological nuclear TDP-43 but identifies only pathological brain lesions^{38,39} (Fig. 3F and G and Supplementary Fig. 2G and H). Finally, we performed immunohistochemistry with an antibody that recognizes the N-terminus and the central region of the protein.³⁷ As expected, we found that in PPIA^{+/+} and PPIA^{-/-}

mice the TDP-43 staining is mainly localized in the nucleus, but in the PPIA^{-/-} mice, in many cases, nuclear clearing was observed (Supplementary Fig. 2I).

We concluded that PPIA deficiency induces a clear-cut neuropathological phenotype in the mouse brain, with marked TDP-43

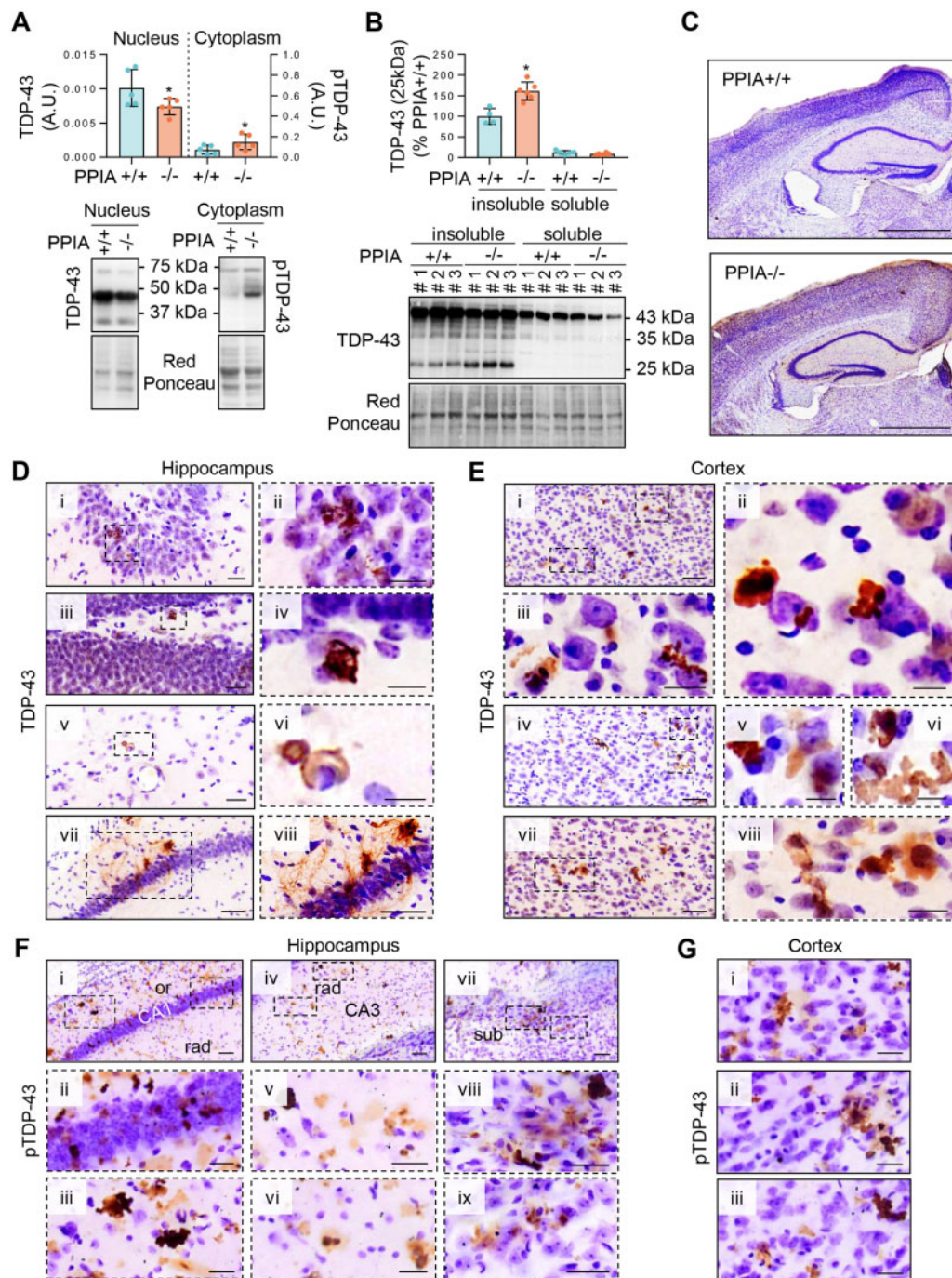


Figure 3 TDP-43 pathology in hippocampus and cortex of PPIA^{-/-} mice. TDP-43 pathology was analysed by biochemical (A and B) and histological (C–G) approaches, at 6 and 12 months. (A) Equal amounts of nuclear and cytoplasmic fractions from cortex of PPIA^{+/+} and PPIA^{-/-} mice were analysed by western blot for TDP-43 (left; AB_2200505) and pTDP-43 (right; AB_1961900). Representative western blots are shown. Data (mean SD; $n = 5$ in each experimental group) indicates the immunoreactivity normalized to total protein loading, in arbitrary units (A.U.); * $P < 0.05$ versus PPIA^{+/+} mice Student's t -test. (B) Representative western blot of TDP-43 (AB_2200505) in soluble and insoluble fractions from cortex of PPIA^{+/+} and PPIA^{-/-} mice and quantification of the 25 kDa TDP-43 fragment are shown. Data (mean SD, $n = 4–6$ in each experimental group) are percentages of immunoreactivity in PPIA^{+/+} insoluble fraction; * $P < 0.05$ versus the PPIA^{+/+} mice by one-way ANOVA, Tukey's post hoc test. (C) Diffuse TDP-43 immunostaining (AB_2200505) was observed in brains of PPIA^{-/-} mice at 12 months compared to PPIA^{+/+}. Scale bar = 1 mm. (D) In hippocampus of PPIA^{-/-} mice, there were TDP-43 inclusions in the pyramidal layer of CA3 and CA1 (1–2), in the granule cell layer of dentate gyrus (3–4), in stratum radiatum of CA1 (5–6) and in stratum oriens of CA3 and CA1 (7–8). D(ii, iv, vi and viii) are magnified images of the dashed area in D(i, iii, v and vii), respectively. Scale bar = 50 μ m in D(vii and viii); 25 μ m in D(i, iii and v); 20 μ m in D(ii); 10 μ m in iv and vi. (E) PPIA^{-/-} mice had TDP-43 inclusions in the somatosensory (1–6) and temporal cortex (7–8). E(ii, iii, v, vi and viii) are magnified images of the dashed area in E(i, iv and vii). Scale bar = 50 μ m in E(i, iv and vii); 20 μ m in E(ii and viii); 10 μ m in E(iii, v and vi). (F and G) pTDP-43 immunostaining (AB_1961900) was analysed in hippocampus (F) and cortex (G) of PPIA^{-/-} mice and control PPIA^{+/+} mice (Supplementary Fig. 2G and H) at 12 months. (F) pTDP-43 inclusions are widespread in the CA1 pyramidal layer (1–2), stratum oriens (or) of CA1 (3), stratum radiatum (rad) of CA3 (4–6) and subiculum (sub) (7–9). F(ii, iii, v, vi, viii and ix) are magnified images of the dashed area in F(i, iv and vii). Scale bar = 50 μ m in F(i, iv and vii); 25 μ m in F(v, viii and ix); 20 μ m in F(ii, iii and vi). (G) pTDP-43 staining was observed in the somatosensory (i) and auditory-temporal (ii and iii) cortex. Scale bar = 20 μ m.

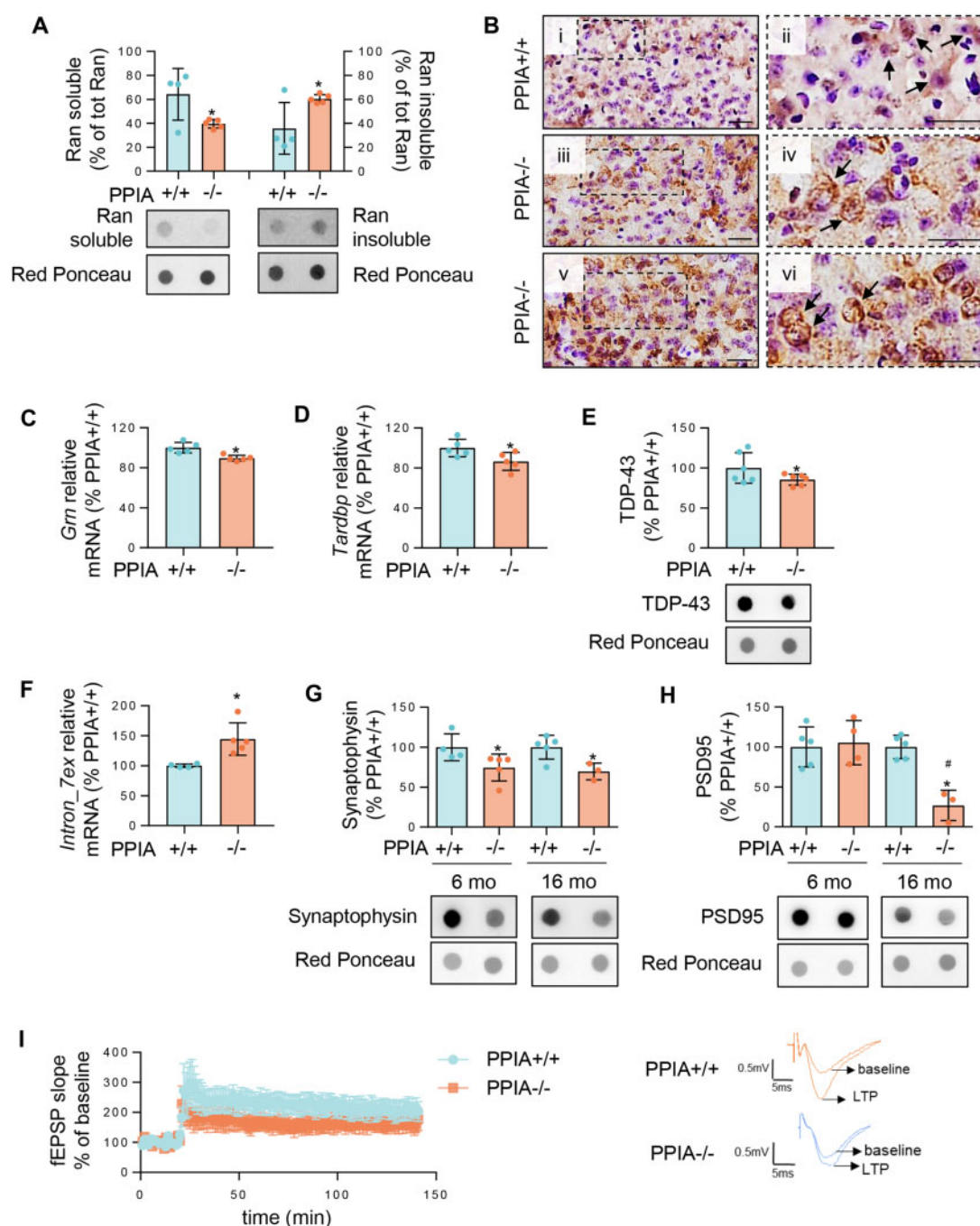


Figure 4 PPIA deficiency affects proteins involved in nucleocytoplasmic transport, TDP-43 autoregulation and synaptic function. (A) Dot blot analysis for Ran-soluble and -insoluble protein in cortex of PPIA^{+/+} and PPIA^{-/-} mice at 6 months of age. Data (mean SD; n = 4 or 5 in each experimental group) are normalized to protein loading and expressed as percentages of total protein, of Ran in soluble and insoluble fractions. Representative dot blots are shown. (B) Ran immunostaining in somatosensory cortex of PPIA^{+/+} [B(i and ii)] and PPIA^{-/-} [B(iii-vi)] mice at 6 months of age. Ran in PPIA^{+/+} mice is mainly nuclear [B(ii) arrows], while in PPIA^{-/-} mice is present also in the cytoplasm [B(iv) arrows], and occasionally forms perinuclear inclusions [B(vi) arrows]. B(ii, iv and vi) are magnified images of the dashed area in B(i, iii and v). Scale bar = 25 μ m. (C-E) Real-time PCR for *Grn* (C) and *Tardbp* (D) mRNA transcripts and dot blot analysis for TDP-43 total protein (AB_2200505) (E), in cortex of PPIA^{+/+} and PPIA^{-/-} mice at 6 months. (C and D) Data (mean SD; n = 5) are normalized to β -actin and expressed as percentages of PPIA^{+/+} relative mRNA. (E) Data (mean SD, n = 6) are normalized to protein loading and are percentages of immunoreactivity in PPIA^{+/+} mice. Representative dot blots are shown. (F) Real-time PCR for *Tardbp* intron 7 exclusion in cortex of PPIA^{+/+} and PPIA^{-/-} mice at 6 months. Data (mean SD; n = 4 or 5 in each experimental group) are normalized to β -actin and expressed as percentages of PPIA^{+/+} relative mRNA; (A and C-E) * P \leq 0.05 versus PPIA^{+/+} mice, Student's t-test. (G and H) Dot blot analysis of synaptophysin (G) and PSD95 (H) in cortex of PPIA^{+/+} and PPIA^{-/-} mice at 6 and 16 months. Immunoreactivity was normalized to protein loading. Representative dot blots are shown. Data (mean SD, n = 3 or 5 in each experimental group) are percentages of immunoreactivity in PPIA^{+/+} mice; * P < 0.05 versus PPIA^{+/+} mice and # P < 0.05 versus 6 months, by one-way ANOVA, uncorrected Fisher's LSD post hoc test (G) and Tukey's post hoc test (H). (I) CA1 LTP induced with theta burst stimulation was lower in PPIA^{-/-} mice (rectangle) than PPIA^{+/+} mice (circles) at 16 months. Data were analysed with two-way ANOVA for repeated measures, P < 0.05 (n = 6). Representative traces recorded in slices from PPIA^{+/+} and PPIA^{-/-} mice, before and after theta burst stimulation, are shown. fEPSP = field excitatory postsynaptic potential.

pathology and other alterations related to protein and RNA homeostasis, getting worse with age.

PPIA deficiency affects proteins involved in nucleocytoplasmic transport, TDP-43 autoregulation and synaptic function

PPIA is a foldase and a molecular chaperone potentially for a wide range of substrates and interacts with Ran.¹³ TDP-43 requires functional Ran for import into the nucleus and regulates its expression.⁴⁰ In the cortex of PPIA^{−/−} mice, Ran total protein level did not differ from controls (data not shown). However, Ran increased substantially (+69%) in the detergent-insoluble fraction and decreased in the soluble fraction (−38%) (Fig. 4A), accumulated in the cytoplasm and occasionally formed perinuclear inclusions (Fig. 4B), already at 6 months of age. These findings may indicate that depletion of the folding/refolding activity of PPIA is at the basis of the reduced solubility and altered localization of Ran and contributes to defective nucleocytoplasmic transport.

PPIA deficiency affects the expression of a number of TDP-43 RNA targets, including *GRN*.¹³ *GRN* mutations in patients result in haplo-insufficiency and *Grn* knock-out mice present an FTD-like phenotype associated with synaptic dysfunction.⁴¹ We verified whether knocking out PPIA influenced *Grn* expression in the brain cortex of the mice. *Grn* mRNA levels were slightly but significantly lower in PPIA^{−/−} mice than controls (Fig. 4C). Surprisingly, TDP-43 at mRNA and protein levels was also lower in PPIA^{−/−} mice than controls (Fig. 4D and E). TDP-43 adjusts its own expression by binding sequences within the 3′ UTR of its own transcript, promoting processing of alternative introns (e.g. intron 7) and mRNA destabilization.^{2,3} We found a 45% increase in the exclusion of *Tardbp* intron 7 in PPIA^{−/−} compared to PPIA^{+/+} mice (Fig. 4F). This suggests that PPIA deficiency may also interfere with the mechanism of TDP-43 autoregulation leading to TDP-43 downregulation.

Substantial depletion of *Tardbp* causes *Grn* upregulation^{3,42} (Supplementary Fig. 3A), suggesting that in normal conditions TDP-43 has a destabilizing effect on the *Grn* transcript. In PPIA^{−/−} mice the mild downregulation of *Tardbp* is associated with mild *Grn* downregulation. Similar results were obtained in cell lines by mild TDP-43 silencing (Supplementary Fig. 3B and C), indicating that a different mechanism probably takes place. Further studies are warranted.

Tardbp depletion in brain downregulates genes involved in synaptic function.³ To assess whether *Grn* and *Tardbp* downregulation was associated with synaptic dysfunction, we first measured the levels of synaptophysin and PSD95, markers of pre- and postsynaptic structures, in the cortex of PPIA^{−/−} mice and controls at 6 and 16 months of age (Fig. 4G and H). Both synaptophysin and PSD95 were lower in PPIA^{−/−} than PPIA^{+/+} mice. Next, we made extracellular field recordings of excitatory postsynaptic potentials in the CA1 hippocampal region of PPIA^{−/−} mice at 16 months of age compared to controls. LTP induced with theta burst stimulation had a smaller amplitude in PPIA^{−/−} mice (Fig. 4I), suggesting impairment of synaptic plasticity in the hippocampus.

PPIA^{−/−} mice develop cognitive, behavioural impairments and late-onset motor neuron disease

We checked whether PPIA deficiency, besides compromising neuronal functions, promotes cognitive, behavioural and motor impairments. Since mice on a 129S6/Sv genetic background do not perform well in cognitive tasks,⁴³ C57_PPIA^{−/−} mice were used for these experiments. We first confirmed that also C57_PPIA^{−/−} mice display TDP-43 pathology (Supplementary Fig. 4). Next, we found that C57_PPIA^{−/−} mice showed no exploratory abnormalities, as

they spent the same time as C57_PPIA^{+/+} mice in the inner zone in the open field test, at both 6 and 12 months of age (Fig. 5A). In the elevated-plus maze paradigm C57_PPIA^{−/−} mice showed less anxiety and more disinhibition as they spent twice the time in the open arms compared with controls (Fig. 5B). This behaviour is lost with time.

We used the three-chamber test to examine sociability and social memory in C57_PPIA^{−/−} mice. C57_PPIA^{−/−} mice at 6 months spent twice the time of controls sniffing the stranger than the empty cage (Fig. 5C), suggesting a more social attitude. However, at 12 months C57_PPIA^{−/−} mice behaved differently, spending the same time with the stranger and the empty cage and significantly less time sniffing the stranger compared with mice at 6 months.

Combining the results of the elevated-plus maze and the three-chamber tests suggests that the greater social attitude of C57_PPIA^{−/−} mice may be the consequence of greater disinhibition. During the social recognition memory task, which requires normal hippocampal function, C57_PPIA^{−/−} mice at 6 months distinguished the stranger mouse (Stranger 2) from the familiar one (Stranger 1) (Fig. 5D), suggesting a normal social memory. However, at 12 months they no longer did it, suggesting social impairment and hippocampal dysfunction.

To investigate the role of impaired hippocampus in C57_PPIA^{−/−} mice further, we used the Morris water maze and novel object recognition tests. C57_PPIA^{−/−} and control mice showed no differences (Fig. 5E and F), suggesting no memory impairment. However, these tests were developed to study Alzheimer's disease-related memory defects in mice and specific tests for FTD are not available.⁴⁴ Furthermore, FTD patients also show mild memory impairments despite the hippocampal degeneration.⁴⁵

At 12 months C57_PPIA^{−/−} mice had lower locomotor speed (Fig. 5G). In PPIA^{−/−} mice, there was no evident motor impairment, as detected by rotarod and a grid test throughout the lifespan (Supplementary Fig. 5A and B). However, at 12 months PPIA^{−/−} mice had mild muscle atrophy (Fig. 5H), from 16 months impaired extension reflex (Fig. 5I) and from 21 months loss of body weight (Fig. 5J). These results correlated with gradual loss of motor neurons in the lumbar spinal tract of PPIA^{−/−} mice, which became significant in the final stage of the disease (Fig. 5K). Finally, there was >4 months shorter survival of PPIA^{−/−} mice than PPIA^{+/+} mice (702 90 days versus 837 107 days) (Fig. 5L).

In summary, mice knock-out for PPIA present cognitive, behavioural and motor impairments reminiscent of ALS-FTD in patients.

Identification of a PPIA loss-of-function mutation in a patient with sporadic ALS

We identified an ALS patient with a heterozygous PPIA missense mutation (NM_021130:c.226A>G.; p.K76E) in an evolutionarily conserved region of the protein (Fig. 6A). To our knowledge, the PPIA: p.K76E is a novel variant absent in the large population dataset gnomAD v2.1.1, in our internal control cohort of 677 healthy participants, matched by age and ancestry, and in the large ALS/FTD dataset ProjectMine (<http://databrowser.projectmine.com/>). The patient had difficulty walking at age 56 and slowly progressed to weakness and spasticity of the lower limbs. Neurological examination revealed increased deep tendon reflex in all extremities and pathological reflexes, including bilateral Hoffman sign and Babinski sign. No additional neurological or systemic abnormalities were detected. The EMG showed signs of lower motor neuron involvement in the upper and lower limbs. Genetic screening for mutations in the most common ALS genes and in a large panel of hereditary spastic paraplegia genes was negative. Appropriate investigations excluded other diseases, and motor impairment

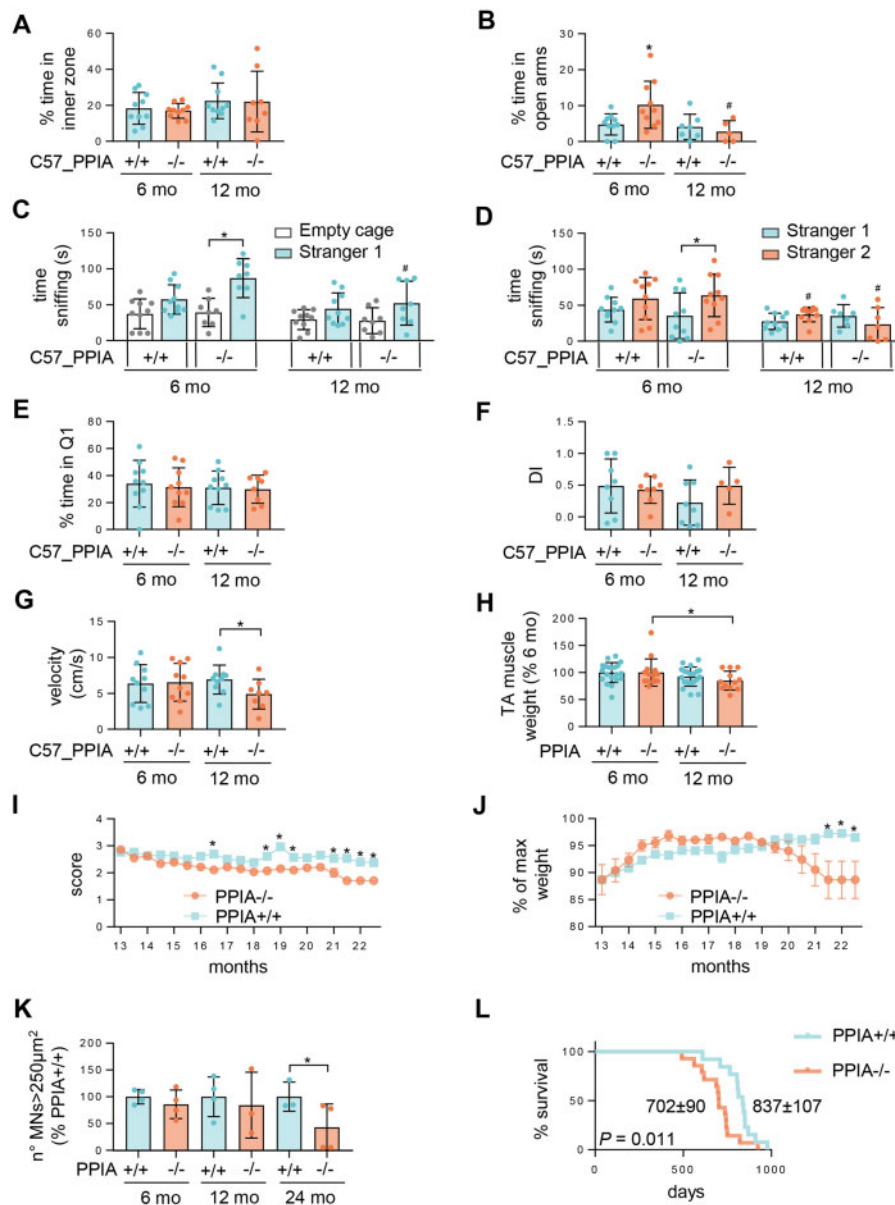


Figure 5 PPIA^{-/-} mice present cognitive, behavioural and motor function deficits. (A) Open field: C57_PPIA^{+/+} and PPIA^{-/-} mice spent similar time in the inner zone both at 6 ($n = 10$) and 12 months of age ($n = 10$ C57_PPIA^{+/+}, $n = 8$ C57_PPIA^{-/-}). (B) Elevated-plus maze: C57_PPIA^{-/-} mice spent more time than controls in open arms ($n = 10$ C57_PPIA^{+/+} and PPIA^{-/-} at 6 months, $n = 7$ C57_PPIA^{+/+} and $n = 5$ C57_PPIA^{-/-} at 12 months) at 6, but not at 12 months of age. (C and D) Three-chamber sociability test. In the sociability trial (C), C57_PPIA^{-/-} mice spent more time than controls sniffing Stranger 1 than empty cage at 6, but not 12 months of age ($n = 10$ C57_PPIA^{+/+}, $n = 8$ C57_PPIA^{-/-}). In the social memory trial (D), C57_PPIA^{-/-} mice spent more time sniffing Stranger 2 than Stranger 1, compared to controls, at 6 ($n = 10$), but not at 12 months ($n = 10$ C57_PPIA^{+/+}, $n = 7$ C57_PPIA^{-/-}). (E) Morris water maze: C57_PPIA^{-/-} and PPIA^{+/+} mice spent a similar time in the target quadrant (Q1) both at 6 ($n = 10$) and 12 ($n = 10$ C57_PPIA^{+/+}, $n = 8$ C57_PPIA^{-/-}) months. (F) Novel object recognition test: C57_PPIA^{+/+} and PPIA^{-/-} mice had similar discrimination indexes (DI) at 6 ($n = 8$) and 12 ($n = 8$ C57_PPIA^{+/+}, $n = 5$ C57_PPIA^{-/-}) months of age. (A–F) Mean \pm SD; * $P \leq 0.05$ versus the PPIA^{+/+} mice and * $P < 0.05$ versus the 6-month-old control by one-way ANOVA, Tukey's post hoc test (A–C, E and F) and uncorrected Fisher's LSD post hoc test (D). (G) Velocity measurement: C57_PPIA^{+/+} and PPIA^{-/-} mice had the same velocity in the open field test at 6 months ($n = 10$) but at 12 months ($n = 10$) but at 12 months ($n = 10$ C57_PPIA^{+/+}, $n = 8$ C57_PPIA^{-/-}) had slower velocity than controls. Data are mean \pm SD and are expressed in cm/s; there was no difference among groups by one-way ANOVA; * $P \leq 0.05$ by Student's *t*-test. (H) PPIA^{-/-} mice show mild atrophy of tibialis anterior (TA) muscle at 12 months ($n = 20$ PPIA^{+/+}, $n = 14$ PPIA^{-/-} at 6 months, $n = 12$ PPIA^{-/-} at 12 months). Data (mean \pm SD) are muscle weights as percentage of 6-month-old control; there was no difference among groups by one-way ANOVA; * $P \leq 0.05$ by Student's *t*-test. (I) Extension reflex: PPIA^{-/-} mice had less extension of hindlimbs than controls ($n = 13$ PPIA^{+/+}, $n = 14$ PPIA^{-/-}). Mean \pm SEM; * $P < 0.05$ by two-way ANOVA, Bonferroni's post hoc test. (J) PPIA^{-/-} mice had greater weight loss than controls from 21 months ($n = 13$ PPIA^{+/+}, $n = 14$ PPIA^{-/-}). Mean \pm SEM; * $P < 0.05$ by two-way ANOVA, Bonferroni's post hoc test. (K) Quantification of Nissl-stained motor neurons (MNs $> 250 \mu\text{m}^2$) in lumbar spinal cord hemisections from PPIA^{+/+} and PPIA^{-/-} mice at 6, 12 and 24 months. Data are mean \pm SD ($n = 3$ or 4 in each experimental group) and are percentages of PPIA^{+/+} mice; there was no difference among groups by one-way ANOVA; * $P \leq 0.05$ by Student's *t*-test. (L) Kaplan–Meier curve for survival of PPIA^{+/+} ($n = 13$) and PPIA^{-/-} mice ($n = 14$). Log-rank Mantel–Cox test for comparing PPIA^{+/+} and PPIA^{-/-} mice.

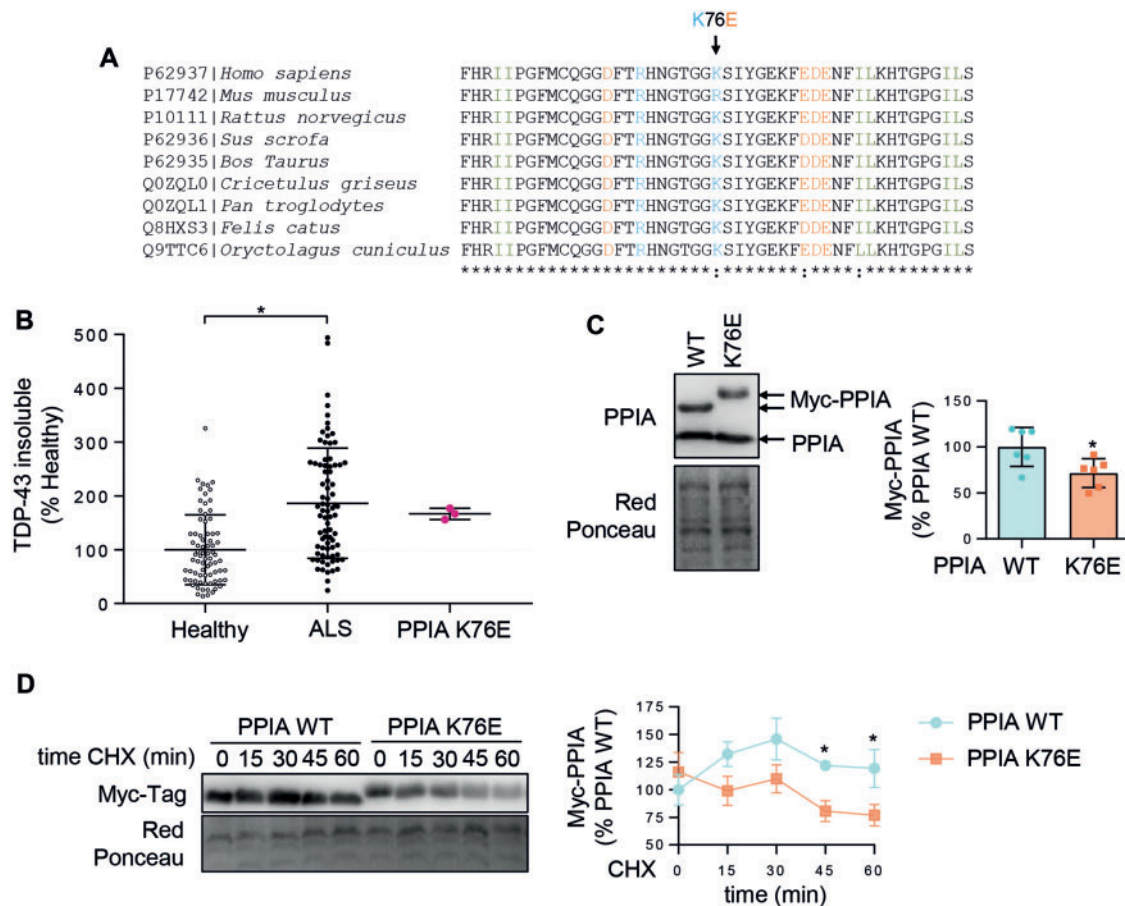


Figure 6 PPIA K76E mutant identified in a patient with sporadic ALS. (A) PPIA is evolutionarily highly conserved, 89% of the amino acid residues are identical in all the species listed. Multiple sequence alignment of PPIA, focused on the mutated lysine in position 76 and surrounding residues, is shown. The asterisk indicates conserved sites; the colon indicates conservative replacements (amino acids with similar biochemical properties); acidic residues (D, E) are in orange, basic residues (K, R) in blue, small aliphatic residues (I, L) in green, all other residues in grey. (B) Slot blot analysis of TDP-43 insoluble protein levels was done in PBMCs from the PPIA K76E ALS patient and compared to TDP-43 insoluble levels from ALS patients and healthy participants of a retrospective cohort (Cohort 1, [Supplementary Table 1](#)). Immunoreactivity of the PPIA K76E patient was normalized to total protein loading and to the internal standard of the retrospective cohort,⁷ to compare the two analyses. Scatter dot plot (mean SD; $n = 76$ healthy controls, $n = 79$ ALS patients and $n = 3$ technical replicates of the PPIA K76E ALS patient) are percentages of healthy controls and dotted line indicates the median value of healthy controls; $P < 0.05$ versus healthy controls, by one-way ANOVA, Tukey's post hoc test. (C) PPIA protein level was lower in HEK293 cells transfected with PPIA K76E mutant than PPIA WT plasmid, after 48 h in culture. Immunoreactivity was normalized to protein loading. Representative western blots are shown. Data (mean SD; $n = 6$) are percentages of PPIA WT; $P < 0.05$ versus PPIA WT Student's *t*-test. (D) PPIA protein level was lower in HEK293 cells transfected with PPIA K76E mutant than PPIA WT plasmid after treatment with 100 μ g/ml cycloheximide (CHX) for 0, 15, 30, 45 and 60 min. Immunoreactivity was normalized to protein loading. Representative western blots are shown. Data (mean SEM; $n = 4$) are percentages of PPIA WT; $P < 0.05$ versus PPIA WT, by one-way ANOVA, uncorrected Fisher's LSD post hoc test. WT = wild-type.

progressed over time. He was diagnosed with ALS at age 59. Cognitive testing was normal. No weakness in the upper limbs or bulbar and respiratory symptoms was reported after 5 years. The patient reported no family history of neurodegenerative disease, psychiatric disease or walking impairment.

We analysed TDP-43 partitioning in PBMCs as a surrogate marker of TDP-43 pathology and found that in the mutant PPIA patient TDP-43 accumulated in the insoluble fraction like the sporadic ALS and ALS-FTD patients of the retrospective cohort (Fig. 6B; Cohort 1, [Supplementary Table 1](#)), confirming the diagnostic value of this parameter in PBMCs.⁷ TARDBP mRNA levels in the PPIA mutant patient were higher than in healthy controls and other ALS patients, while the protein level tended to be lower than the retrospective cohort ([Supplementary Fig. 6C and D](#)).

Known PPIA variants have low protein stability and are rapidly degraded.⁴⁶ We hypothesized that PPIA K76E could be a loss-of-function variant. We transfected HEK293 cells with myc-tagged wild-type PPIA (PPIA WT) and K76E and detected a lower level of

the exogenous mutant protein than in wild-type after 48 h in culture (Fig. 6C), despite equivalent transfection, as detected in parallel wells by western blot with anti-myc antibody after 24 h in culture (Fig. 6D, time point 0). The lower stability of the mutant protein was confirmed by the accelerated degradation over time in cells treated with an inhibitor of new protein synthesis (Fig. 6D). Moreover, PPIA total protein levels in PBMCs were lower in the PPIA mutant patient than in the retrospective cohort⁷ of healthy participants (~33%) and ALS patients (~16%) ([Supplementary Fig. 6A](#)). PPIA mRNA levels, however, were higher in the mutant PPIA patient than in other ALS patients, although lower than in healthy controls ([Supplementary Fig. 6B](#)).

We also examined possible structural differences between PPIA WT and K76E by molecular dynamics simulations (Fig. 7 and [Supplementary Fig. 7](#)). The analysis identified two regions (residues 26–30 and 43–45) outlining α -helix 1 in which the conformation of PPIA K76E significantly differed from the wild-type form (Fig. 7A and B). The mutant protein the 43–45 loop is significantly

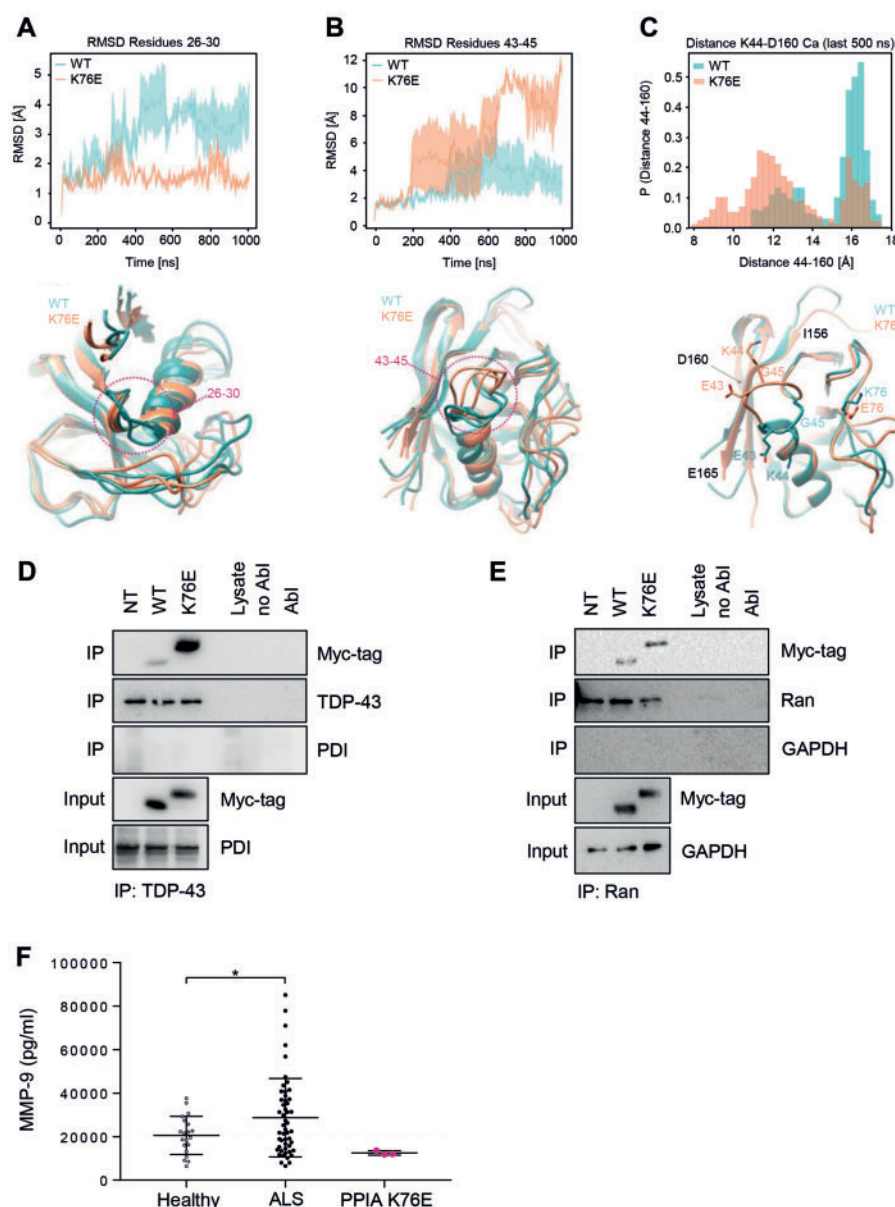


Figure 7 PPIA K76E shows structural differences from wild-type and is a loss-of-function mutant. (A and B) Structural analysis of protein loops composed residues 26–30 (A) and residues 43–45 (B) by molecular dynamics simulation. The protein root mean square deviation (RMSD) of each frame, computed in comparison to the initial conformation, is plotted as a function of the simulation time [wild-type (WT) blue, K76E orange]. Lines and filled curves represent the mean and standard error of the RMSD, respectively, computed for the three replicates of the wild-type and mutant protein. A significant difference between the two variants in loop 26–30 is evident after 400 ns of simulations (A); in the loop 43–45, the difference is clear after 700 ns (B). Three molecular dynamics snapshots sampled at the end of the simulations for the wild-type protein (blue) superimposed on three molecular dynamics snapshots sampled at the end of the simulations for the K76E variant (orange) are presented below the relative graph. (C) A detail of the structural variation of loop 43–45, with the probability distribution, computed considering the last 500 ns of dynamics, of the C α distance between the residue at the centre of the 43–45 loop (lysine 44) and the residue in the centre of the β -strand 156–165 (aspartate 160). In the simulations of the K76E variant, the loop spent significantly more time closer to the β -strand 156–165 than the wild-type. The side-chains of the loop-residues face opposite directions in the two protein variants, as shown with representative conformations sampled after 1 μ s of molecular dynamics and superimposed below the graph. Here side-chains of residues E43, K44, G45 and K/E76 are explicitly represented (WT blue, K76 orange), while the positions of residues I156, D160 and E165 are indicated in grey. (D and E) Cells were transfected with PPIA WT or PPIA K76E construct, or not transfected (NT). TDP-43 (D) or Ran (E) was co-immunoprecipitated from cells using an anti-TDP-43 polyclonal antibody (AB_2200505) or anti-Ran polyclonal antibody, respectively, followed by anti-Myc western blot. Controls for immunoprecipitation (IP) experiments: lysate, lysate with magnetic beads linked to the secondary antibody (beads-IgGII); no AbI, lysis buffer with beads-IgGII; AbI, lysis buffer with beads-IgGII and primary antibody. Western blot anti-TDP-43 (AB_425904) and anti-Ran show an equal amount of IPed TDP-43 or Ran in PPIA WT, PPIA K76, NT cells. Western blot anti-PDI (D) and anti-GAPDH (E), performed as negative controls respectively of TDP-43 and Ran co-immunoprecipitations, show no signal in immunoprecipitation fraction and an immunosignal in input fraction. Representative western blots are shown. (F) AlphaLISA analysis of MMP-9 was done in plasma samples from the PPIA K76E ALS patient, ALS patients and healthy participants (Cohort 3, [Supplementary Table 1](#)). Scatter dot plots are mean \pm SD (n = 20 healthy controls, n = 51 ALS patients and n = 3 technical replicates of the PPIA K76E ALS patient). The dotted line indicates the median of healthy controls; * P < 0.05 by one-way ANOVA, uncorrected Fisher's LSD post hoc test.

closer to the nearby β -strand (residues 156–165) (Fig. 7C). Since the K76E mutation lies within a coil in direct contact with helix-1, this suggested that the effect of the mutation is not only limited to a local change of electrostatic properties, but could instead result in a structural alteration of nearby regions essential for catalytic activity and protein interaction.⁴⁷ PPIA has a wide interaction network.¹³ We tested whether the mutation impaired PPIA interaction with TDP-43 and Ran by co-immunoprecipitation (Fig. 7D and E). We found that both TDP-43 and Ran have an aberrant interaction with PPIA K76E, with a substantial increase in the affinity of both proteins for the mutant PPIA compared to PPIA WT.

The extracellular form of PPIA is toxic for motor neurons by activating the EMMPRIN/CD147 receptor and inducing MMP-9 expression.¹⁸ We measured MMP-9 plasma levels in the mutant PPIA patient and in a cohort of ALS patients and healthy participants (Fig. 7F; Cohort 3, Supplementary Table 1). While ALS patients had a higher level of MMP-9 than healthy controls, the PPIA mutant patient had one of the lowest levels of MMP-9, also suggesting a reduced toxic extracellular function of PPIA.

We conclude that K76E is a loss-of-function mutation that may affect both intracellular protective and extracellular toxic PPIA functions, leading to ALS with a slowly progressive phenotype in the patient. Further studies directly testing the function of mutant PPIA are necessary to dissect all possible implications.

Discussion

TDP-43 proteinopathy is a prominent neuropathological feature in the ALS/FTD disease spectrum that is also seen in a wide range of neurodegenerative diseases, inherited and sporadic.⁴ Neither the factors driving TDP-43 pathology nor its involvement in neurodegeneration have been defined yet. We propose that defective PPIA is a key factor in the cytoplasmic mislocalization and aggregation of TDP-43, induces neurodegeneration and is a common feature in ALS/FTD patients.

PPIA is an evolutionarily conserved foldase and molecular chaperone, abundant in the cytoplasm but also present in the nucleus.^{7,12} Its PPIase activity has been regarded as fundamental in protein folding and refolding especially under stress conditions.^{13–15} PPIA was found entrapped in aggregates isolated from spinal cord and brain of ALS/FTD patients and mouse models while exerting its protective function against misfolding.^{20,48} However, the absence of an overt phenotype in the PPIA^{−/−} mouse in the work of Colgan et al.^{24,25} and its dispensable function in mammalian cells have kept its physiological role enigmatic, especially in the CNS where it is highly expressed.

In a previous work characterizing the protein interacting network of PPIA under basal conditions we found that it includes several proteins involved in RNA homeostasis, hnRNPs and TDP-43.¹³ We also reported that PPIA regulates key TDP-43 functions, such as gene expression regulation.¹³ In fact, knocking down PPIA affected the expression of TDP-43 RNA targets implicated in FTD/ALS, such as GRN, VCP and FUS, or in protein clearance, such as HDAC6 and ATG7. As a consequence, the mutant SOD1 mouse cross-bred with the PPIA^{−/−} mouse had a more severe disease phenotype, with more protein aggregation and less survival. Besides SOD1, TDP-43 and hnRNPs,¹³ PPIA interacts with other proteins linked to genetic forms of ALS/FTD, such as ubiquilin 2,⁴⁹ and Arg-containing dipeptide repeat proteins.⁵⁰ We therefore concluded that PPIA could be a modifier of ALS/FTD pathology.

In this work, we demonstrate that the loss of PPIA in mice is sufficient to induce neurodegeneration leading to a clinical phenotype of the ALS/FTD spectrum. We also show that PPIA is defective in several ALS and ALS-FTD patients and that a participant carrying a loss-of-function PPIA mutation develops ALS. Therefore,

besides the general intracellular protective effect under stress, we provide evidence that PPIA has specific, non-redundant functions that are particularly relevant for TDP-43 biology.

Deficient PPIA alters the biochemical properties and localization of Ran, and this may underlie the impaired TDP-43 nuclear import. Ran is a master regulator of the nuclear protein import and is required for most of the proteins that shuttle between the nucleus and cytoplasm. Non-functional Ran reduced TDP-43 nuclear localization in cortical neurons.⁴⁰ Ran is also a PPIA interactor¹³ and has a GP-motif (residues 57–58), the recognition site for the foldase activity of PPIA, present also in TDP-43 and other PPIA substrates.^{13,47,51,52} In the absence of PPIA, Ran forms inclusions in the mouse brain. Ran and other regulators of nucleocytoplasmic trafficking accumulate in the cytoplasm of ALS/FTD cellular models,^{53–55} either as demixed droplets or in stress granules, suggesting that defective PPIA may have a role in the pathogenic mechanisms that couple cellular stress with impaired nucleocytoplasmic transport. Biochemical analysis of the detergent-insoluble fraction of the cortex of PPIA^{−/−} mice did in fact indicate a general increase in insoluble proteins and TIA1 stress granule marker.

Defective PPIA alters TARDBP mRNA expression. In PPIA^{−/−} mice *Tardbp* mRNA is downregulated, and in the mutant PPIA patient it is upregulated. TDP-43 physiological levels are tightly controlled at a transcriptional level by an autoregulatory loop, which keeps intracellular TDP-43 within a narrow range.^{2,3} This is necessary, for example, for TDP-43's role in RNP complexes that may become dysfunctional if the stoichiometry between TDP-43 and the other protein/RNA components is disrupted.¹³ In a previous work, we demonstrated that PPIA through its foldase activity affects the binding of TDP-43 to RNA.¹³ Therefore, we can assume that in absence of PPIA increased *Tardbp* intron 7 splicing and consequent *Tardbp* mRNA destabilization in mice may be caused by an anomalous interaction of TDP-43 with its 3' UTR. In the patient with the mutation, we can hypothesize that PPIA K76E, that has an aberrant interaction with TDP-43, sequesters TDP-43 and affects autoregulation in the opposite direction, promoting the production of stable mRNA species.⁵⁶ Further studies are needed to decipher the exact mechanism at the basis of these divergent effects at an mRNA level, while at a protein level in both cases TDP-43 decreases. It is of relevance that PPIA is widely implicated in RNA biology. It interacts not only with TDP-43, but also with several other proteins involved in mRNA processing and transport and itself is an mRNA binding protein.^{13,57} Therefore, we can hypothesize that defective PPIA function may affect at multiple levels TDP-43 post-transcriptional regulation.

If complete ablation of TDP-43 is embryonically lethal, conditional knock-out and limited knock-down of TDP-43 results in neurodegeneration.^{58,59} Moreover, TDP-43 depletion in brain downregulates genes with very long introns that encode proteins involved in synaptic function.^{3,60} In agreement with this, we detected downregulation of synaptic proteins and impairment of synaptic plasticity in the hippocampus of PPIA^{−/−} mice, indicating that PPIA deficiency also has an effect on synaptic structure and function.

In several pathological conditions, oxidative stress and inflammation increase PPIA secretion into biofluids.⁶¹ The levels of PPIA were high in the CSF of ALS patients and mutant SOD1 rodent models.¹⁸ Once secreted, PPIA activates a proinflammatory pathway by the EMMPRIN/CD147 receptor, leading to NF- κ B activation and induction of MMP-9 expression in neurons and glia.¹⁸ Large, fast-twitch, fatigable α motor neurons, which are the most susceptible to degeneration in ALS, express the highest level of MMP-9, which enhances endoplasmic reticulum stress and promotes neurodegeneration.⁶² High levels of MMP-9 in tissues and biofluids of ALS patients have been detected in this work and by other

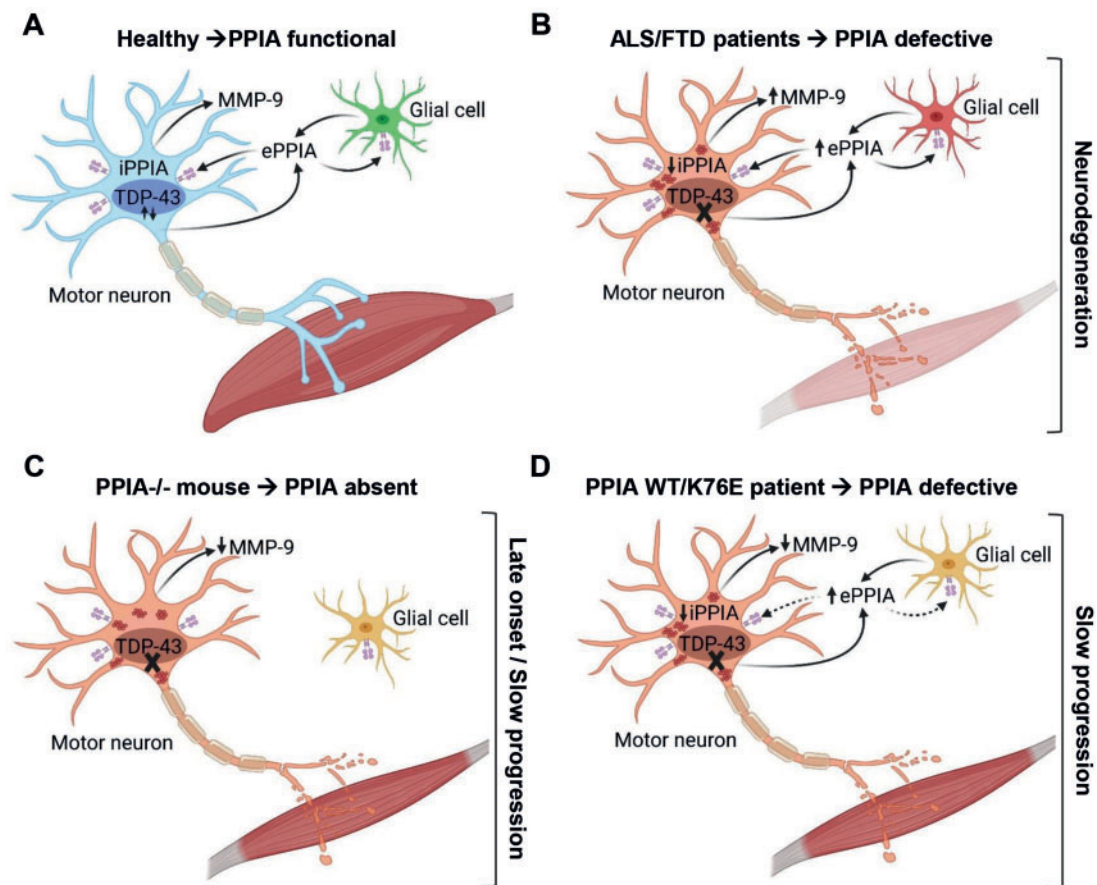


Figure 8 Schematic representation of PPIA function in physiological and pathological conditions. (A) PPIA (iPPIA) is highly expressed in neurons and motor neurons where it is protective thanks to its activity as a foldase and molecular chaperone that affects key proteins involved in RNA metabolism, nucleocytoplasmic transport and synaptic function. PPIA is secreted (ePPIA) in response to oxidative stress and inflammatory stimuli.⁶¹ (B) In ALS/FTD, defective iPPIA induces TDP-43 pathology, nucleocytoplasmic transport defects, synaptic dysfunction and neurodegeneration. Persistent cellular stress in neurons and glia leads to aberrant secretion of PPIA that, through the interaction with its EMMPRIN/CD147 receptor, induces MMP-9 expression and an inflammatory response which is particularly toxic for motor neurons.^{18,62} (C and D) In the PPIA^{-/-} mouse (C) and PPIA WT/K76E patient (D), the detrimental effect of deficient iPPIA function is partially compensated by the lack (mouse) or lower (patient) ePPIA-induced inflammatory response, leading to marked TDP-43 pathology associated with late-onset/slowly progressive (mouse) or slowly progressive (patient) motor neuron disease.

groups^{63,64} and has been associated with blood–brain barrier breakdown.⁶⁵ We previously reported that selective pharmacological inhibition of extracellular PPIA (ePPIA) reduced MMP-9, promoted a prohealing phenotype in glia, rescued motor neurons and increased survival in the SOD1 G93A mouse model of ALS.¹⁸ We also showed that ePPIA was toxic towards motor neurons, which express high levels of EMMPRIN/CD147, but had no effect on cortical and cerebellar granule neurons.¹⁸

The late-onset and slowly progressing motor dysfunction in PPIA^{-/-} mice can be explained with the substantially reduced activation of the EMMPRIN/CD147-dependent proinflammatory pathway to which motor neurons are particularly susceptible (Fig. 8). In the patient heterozygous for mutant PPIA, half the ePPIA may be unable to activate EMMPRIN/CD147, reducing neuroinflammation and slowing progression of the disease. Defective intracellular PPIA (iPPIA) increases cellular stress, ultimately leading to PPIA secretion. We hypothesize a tug-of-war between iPPIA and ePPIA, in which the prevalence of ePPIA over iPPIA accelerates disease progression. Increasing iPPIA function may reduce ePPIA and be an effective therapeutic approach.

Several mouse models of ALS/FTD have been generated targeting genes with known pathogenic roles but each one recapitulates only certain aspects of the human disease. For instance, TDP-43

pathology in mice is often absent or mild and is not always linked to neurodegeneration or behavioural phenotypes.⁶⁶ In TDP-43 mouse models overexpressing wild-type TDP-43 or disease-associated mutations, C-terminal TDP-43 fragments are detected at low levels or are absent.⁶⁷ PPIA^{-/-} mice are characterized by diffuse, marked TDP-43 pathology in cortex, hippocampus and spinal cord,¹³ with all the key neuropathological features of ALS/FTD including cytoplasmic mislocalization and accumulation of C-terminal fragments of TDP-43 associated with neurodegeneration and cognitive and behavioural impairments. In PPIA^{-/-} mice, the behavioural symptoms follow a peculiar course. Initially, they present disinhibition with no social impairment, and later they show loss of disinhibition and develop apathy and social disinterest. Interestingly, while most patients with the behavioural variant of FTD (bvFTD) display both disinhibition and apathy during the course of the disease, some may initially present as primarily disinhibited or primarily apathetic and later develop either signs of inertia or disinhibition.⁶⁸ Moreover, despite clear evidence that cognitive/behavioural impairment may appear early in the course of ALS, deterioration does not always seem to occur with disease progression.⁶⁹

There is a significant genetic and neuropathological overlap between ALS and FTD with up to 50% of ALS patients having cognitive and behavioural manifestations and up to 40% of FTD patients

developing motor dysfunction.⁷⁰ However, it is not clear which pathway is at the basis of either phenotype. Interestingly, PPIA^{−/−} mice display early key symptoms of bvFTD and only later develop motor dysfunction. The resulting picture resembles a behaviourally predominant ALS-FTD in which behavioural symptoms typically evolve before motor symptoms.⁷¹ GRN deficiency, the cause of a tau-negative familial form of FTD,⁷² probably contributes to the development of a predominant FTD phenotype in PPIA^{−/−} mice.

PPIA genetic variants are very rare, so individuals homozygous for any of them are even more unlikely.⁴⁶ The identification of a PPIA variant in a single patient cannot definitely demonstrate its causality. However, the structural and functional properties of the mutant protein are suggestive of its possible involvement in disease pathogenesis. More relevant for the disease is the regulation of PPIA at a post-translational level. PPIA is commonly and variably post-translationally modified and these modifications regulate its functions.^{13,21,73,74} The interaction with TDP-43 is favoured by PPIA Lys-acetylation, which is low in ALS patients.¹³ Here we also report downregulated PPIA in two independent cohorts of patients; therefore, we predict that an overall defective PPIA is likely in several patients and needs to be further investigated in large clinical studies.

In conclusion, our findings indicate that PPIA is involved in multiple pathways that protect CNS from TDP-43-mediated toxicity. In fact, if deficient and/or dysfunctional PPIA can trigger TDP-43 proteinopathy leading to neurodegeneration. PPIA^{−/−} mice recapitulate key features of ALS-FTD and are useful experimental model to investigate the mechanisms of TDP-43 proteinopathy, with the aim of developing novel therapeutic approaches.

Acknowledgements

We thank Bradford C. Berk and Patrizia Nigro for providing the PPIA^{−/−} mice on C57BL/6J genetic background and the Laboratory of Neurogenetics (NIH) staff for their collegial support and technical assistance. We thank Judith Baggott for editorial assistance and Fabrizio Aspesi for graphics assistance by BioRender.com.

Funding

This work was supported by grants from the ‘Fondazione Regionale per la Ricerca Biomedica di Regione Lombardia’, project TRANS-ALS (to V.B.), ERA-Net for Research Programmes on Rare Diseases, project MAXOMOD (to V.B.), the Italian Ministry of Health, project RF-2018–12365614 (to A.C. and V.B.) and RF-2013–02356221 (to V.B.), and in part by the Intramural Research Program of the National Institutes of Health (1ZIAAG000935). S.P. is the recipient of the 2019 Marlene Reimer Brainstar of the year award from CIHR-CAN (ICT-171454).

Competing interests

B.J.T. is an editorial board member for the *Journal of Neurology, Neurosurgery and Psychiatry* and *Neurobiology of Aging* and is an associate editor for *Brain*. All other authors report no competing interests.

Supplementary material

Supplementary material is available at *Brain* online.

References

- Ratti A, Buratti E. Physiological functions and pathobiology of TDP-43 and FUS/TLS proteins. *J Neurochem*. 2016;138 (Suppl 1): 95–111.
- Ayala YM, De Conti L, Avendaño-Vázquez SE, et al. TDP-43 regulates its mRNA levels through a negative feedback loop. *EMBO J*. 2011;30(2):277–288.
- Polymenidou M, Lagier-Tourenne C, Hutt KR, et al. Long pre-mRNA depletion and RNA missplicing contribute to neuronal vulnerability from loss of TDP-43. *Nat Neurosci*. 2011;14(4): 459–468.
- de Boer EMJ, Orié VK, Williams T, et al. TDP-43 proteinopathies: A new wave of neurodegenerative diseases. *J Neurol Neurosurg Psychiatry*. 2020;92(1):86–95.
- Neumann M, Sampathu DM, Kwong LK, et al. Ubiquitinated TDP-43 in frontotemporal lobar degeneration and amyotrophic lateral sclerosis. *Science*. 2006;314(5796):130–133.
- De Marco G, Lupino E, Calvo A, et al. Cytoplasmic accumulation of TDP-43 in circulating lymphomonocytes of ALS patients with and without TARDBP mutations. *Acta Neuropathol*. 2011;121(5): 611–622.
- Luotti S, Pasetto L, Porcu L, et al. Diagnostic and prognostic values of PBMC proteins in amyotrophic lateral sclerosis. *Neurobiol Dis*. 2020;139:104815.
- Guo L, Kim HJ, Wang H, et al. Nuclear-import receptors reverse aberrant phase transitions of RNA-binding proteins with prion-like domains. *Cell*. 2018;173(3):677–692.e20.
- Kim HJ, Taylor JP. Lost in transportation: Nucleocytoplasmic transport defects in ALS and other neurodegenerative diseases. *Neuron*. 2017;96(2):285–297.
- Tziortzouda P, Van Den Bosch L, Hirth F. Triad of TDP43 control in neurodegeneration: Autoregulation, localization and aggregation. *Nat Rev Neurosci*. 2021;22(4):197–208.
- Ryffel B, Woerly G, Greiner B, Haendler B, Mihatsch MJ, Foxwell BM. Distribution of the cyclosporine binding protein cyclophilin in human tissues. *Immunology*. 1991;72(3):399–404.
- Fischer G, Wittmann-Liebold B, Lang K, Kiehlhaber T, Schmid FX. Cyclophilin and peptidyl-prolyl cis-trans isomerase are probably identical proteins. *Nature*. 1989;337(6206):476–478.
- Lauranzano E, Pozzi S, Pasetto L, et al. Peptidylprolyl isomerase A governs TARDBP function and assembly in heterogeneous nuclear ribonucleoprotein complexes. *Brain*. 2015;138(Pt 4): 974–991.
- Lee JP, Palfrey HC, Bindokas VP, et al. The role of immunophilins in mutant superoxide dismutase-1-linked familial amyotrophic lateral sclerosis. *Proc Natl Acad Sci U S A*. 1999;96(6):3251–3256.
- Boulos S, Meloni BP, Arthur PG, Majda B, Bojarski C, Knuckey NW. Evidence that intracellular cyclophilin A and cyclophilin A/CD147 receptor-mediated ERK1/2 signalling can protect neurons against in vitro oxidative and ischemic injury. *Neurobiol Dis*. 2007;25(1):54–64.
- Pan H, Luo C, Li R, et al. Cyclophilin A is required for CXCR4-mediated nuclear export of heterogeneous nuclear ribonucleoprotein A2, activation and nuclear translocation of ERK1/2, and chemotactic cell migration. *J Biol Chem*. 2008;283(1):623–637.
- Sherry B, Yarlett N, Strupp A, Cerami A. Identification of cyclophilin as a proinflammatory secretory product of lipopolysaccharide-activated macrophages. *Proc Natl Acad Sci U S A*. 1992; 89(8):3511–3515.
- Pasetto L, Pozzi S, Castelnovo M, et al. Targeting extracellular cyclophilin A reduces neuroinflammation and extends survival in a mouse model of amyotrophic lateral sclerosis. *J Neurosci*. 2017;37(6):1413–1427.

19. Nigro P, Pompilio G, Capogrossi MC. Cyclophilin A: A key player for human disease. *Cell Death Dis.* 2013;4:e888.
20. Basso M, Samengo G, Nardo G, et al. Characterization of detergent-insoluble proteins in ALS indicates a causal link between oxidative stress and aggregation in pathogenesis. *PLoS One.* 2009;4(12):e8130.
21. Massignan T, Casoni F, Basso M, et al. Proteomic analysis of spinal cord of presymptomatic amyotrophic lateral sclerosis G93A SOD1 mouse. *Biochem Biophys Res Commun.* 2007;353(3):719–725.
22. Nardo G, Pozzi S, Pignataro M, et al. Amyotrophic lateral sclerosis multiprotein biomarkers in peripheral blood mononuclear cells. *PLoS ONE.* 2011;6(10):e25545.
23. Filareti M, Luotti S, Pasetto L, et al. Decreased levels of foldase and chaperone proteins are associated with an early-onset amyotrophic lateral sclerosis. *Front Mol Neurosci.* 2017;10:99.
24. Colgan J, Asmal M, Luban J. Isolation, characterization and targeted disruption of mouse ppia: Cyclophilin A is not essential for mammalian cell viability. *Genomics.* 2000;68(2):167–178.
25. Colgan J, Asmal M, Neagu M, et al. Cyclophilin A regulates TCR signal strength in CD4⁺ T cells via a proline-directed conformational switch in Itk. *Immunity.* 2004;21(2):189–201.
26. Mancini S, Balducci C, Micotti E, et al. Multifunctional liposomes delay phenotype progression and prevent memory impairment in a presymptomatic stage mouse model of Alzheimer disease. *J Controlled Release.* 2017;258:121–129.
27. Pasetto L, Olivari D, Nardo G, et al. Micro-computed tomography for non-invasive evaluation of muscle atrophy in mouse models of disease. *PLoS ONE.* 2018;13(5):e0198089.
28. Nardo G, Trolese MC, de Vito G, et al. Immune response in peripheral axons delays disease progression in SOD1(G93A) mice. *J Neuroinflammation.* 2016;13(1):261.
29. Brooks BR, Miller RG, Swash M, Munsat TL; World Federation of Neurology Research Group on Motor Neuron Diseases. El Escorial revisited: Revised criteria for the diagnosis of amyotrophic lateral sclerosis. *Amyotroph Lateral Scler Mot Neuron Disord.* 2000;1(5):293–299.
30. Iazzolino B, Peotta L, Zucchetti JP, et al. Differential neuropsychological profile of patients with amyotrophic lateral sclerosis with and without C9orf72 mutation. *Neurology.* 2021;96(1):e141–e152.
31. Rascovsky K, Hodges JR, Knopman D, et al. Sensitivity of revised diagnostic criteria for the behavioural variant of frontotemporal dementia. *Brain.* 2011;134(Pt 9):2456–2477.
32. Strong MJ, Abrahams S, Goldstein LH, et al. Amyotrophic lateral sclerosis - frontotemporal spectrum disorder (ALS-FTSD): Revised diagnostic criteria. *Amyotroph Lateral Scler Front Degener.* 2017;18(3–4):153–174.
33. Pettersen EF, Goddard TD, Huang CC, et al. UCSF Chimera—a visualization system for exploratory research and analysis. *J Comput Chem.* 2004;25(13):1605–1612.
34. Lee EB, Lee VM-Y, Trojanowski JQ. Gains or losses: Molecular mechanisms of TDP43-mediated neurodegeneration. *Nat Rev Neurosci.* 2011;13(1):38–50.
35. Josephs KA, Zhang Y-J, Baker M, Rademakers R, Petrucelli L, Dickson DW. C-terminal and full length TDP-43 species differ according to FTLTDP lesion type but not genetic mutation. *Acta Neuropathol Commun.* 2019;7(1):100.
36. Cicardi ME, Cristofani R, Rusmini P, et al. Tdp-25 routing to autophagy and proteasome ameliorates its aggregation in amyotrophic lateral sclerosis target cells. *Sci Rep.* 2018;8(1):12390.
37. Goossens J, Vanmechelen E, Trojanowski JQ, et al. TDP-43 as a possible biomarker for frontotemporal lobar degeneration: A systematic review of existing antibodies. *Acta Neuropathol Commun.* 2015;3:15.
38. Hasegawa M, Arai T, Nonaka T, et al. Phosphorylated TDP-43 in frontotemporal lobar degeneration and amyotrophic lateral sclerosis. *Ann Neurol.* 2008;64(1):60–70.
39. Neumann M, Kwong LK, Lee EB, et al. Phosphorylation of S409/410 of TDP-43 is a consistent feature in all sporadic and familial forms of TDP-43 proteinopathies. *Acta Neuropathol.* 2009;117(2):137–149.
40. Ward ME, Taubes A, Chen R, et al. Early retinal neurodegeneration and impaired Ran-mediated nuclear import of TDP-43 in progranulin-deficient FTLTDP. *J Exp Med.* 2014;211(10):1937–1945.
41. Petkau TL, Neal SJ, Milnerwood A, et al. Synaptic dysfunction in progranulin-deficient mice. *Neurobiol Dis.* 2012;45(2):711–722.
42. Colombrita C, Onesto E, Megiorni F, et al. TDP-43 and FUS RNA-binding proteins bind distinct sets of cytoplasmic messenger RNAs and differently regulate their post-transcriptional fate in motoneuron-like cells. *J Biol Chem.* 2012;287(19):15635–15647.
43. Brooks SP, Pask T, Jones L, Dunnett SB. Behavioural profiles of inbred mouse strains used as transgenic backgrounds. II: Cognitive tests. *Genes Brain Behav.* 2005;4(5):307–317.
44. Vernay A, Sellal F, René F. Evaluating behavior in mouse models of the behavioral variant of frontotemporal dementia: Which test for which symptom? *Neurodegener Dis.* 2016;16(3–4):127–139.
45. de Souza LC, Chupin M, Bertoux M, et al. Is hippocampal volume a good marker to differentiate Alzheimer's disease from frontotemporal dementia? *J Alzheimers Dis.* 2013;36(1):57–66.
46. von Hahn T, Ciesek S. Cyclophilin polymorphism and virus infection. *Curr Opin Virol.* 2015;14:47–49.
47. Howard BR, Vajdos FF, Li S, Sundquist WI, Hill CP. Structural insights into the catalytic mechanism of cyclophilin A. *Nat Struct Biol.* 2003;10(6):475–481.
48. Seyfried NT, Gozal YM, Donovan LE, et al. Quantitative analysis of the detergent-insoluble brain proteome in frontotemporal lobar degeneration using SILAC internal standards. *J Proteome Res.* 2012;11(5):2721–2738.
49. Blokhuis AM, Koppers M, Groen EJM, et al. Comparative interactomics analysis of different ALS-associated proteins identifies converging molecular pathways. *Acta Neuropathol.* 2016;132(2):175–196.
50. Lee K-H, Zhang P, Kim HJ, et al. C9orf72 dipeptide repeats impair the assembly, dynamics, and function of membrane-less organelles. *Cell.* 2016;167(3):774–788.e17.
51. Yurchenko V, Zybarch G, O'Connor M, et al. Active site residues of cyclophilin A are crucial for its signaling activity via CD147. *J Biol Chem.* 2002;277(25):22959–22965.
52. Piotukh K, Gu W, Kofler M, Labudde D, Helms V, Freund C. Cyclophilin A binds to linear peptide motifs containing a consensus that is present in many human proteins. *J Biol Chem.* 2005;280(25):23668–23674.
53. Chou C-C, Zhang Y, Umoh ME, et al. TDP-43 pathology disrupts nuclear pore complexes and nucleocytoplasmic transport in ALS/FTD. *Nat Neurosci.* 2018;21(2):228–239.
54. Gasset-Rosa F, Lu S, Yu H, et al. Cytoplasmic TDP-43 de-mixing independent of stress granules drives inhibition of nuclear import, loss of nuclear TDP-43, and cell death. *Neuron.* 2019;102(2):339–357.e7.
55. Zhang K, Daigle JG, Cunningham KM, et al. Stress granule assembly disrupts nucleocytoplasmic transport. *Cell.* 2018;173(4):958–971.e17.
56. White MA, Kim E, Duffy A, et al. TDP-43 gains function due to perturbed autoregulation in a Tardbp knock-in mouse model of ALS-FTD. *Nat Neurosci.* 2018;21(4):552–563.

57. Castello A, Fischer B, Eichelbaum K, et al. Insights into RNA biology from an atlas of mammalian mRNA-binding proteins. *Cell*. 2012;149(6):1393–1406.
58. Iguchi Y, Katsuno M, Niwa J, et al. Loss of TDP-43 causes age-dependent progressive motor neuron degeneration. *Brain*. 2013; 136(Pt 5):1371–1382.
59. Wu L-S, Cheng W-C, Shen C-KJ. Targeted depletion of TDP-43 expression in the spinal cord motor neurons leads to the development of amyotrophic lateral sclerosis-like phenotypes in mice. *J Biol Chem*. 2012;287(33):27335–27344.
60. Sephton CF, Cenik C, Kucukural A, et al. Identification of neuronal RNA targets of TDP-43-containing ribonucleoprotein complexes. *J Biol Chem*. 2011;286(2):1204–1215.
61. Hoffmann H, Schiene-Fischer C. Functional aspects of extracellular cyclophilins. *Biol Chem*. 2014;395(7-8):721–735.
62. Kaplan A, Spiller KJ, Towne C, et al. Neuronal matrix metalloproteinase-9 is a determinant of selective neurodegeneration. *Neuron*. 2014;81(2):333–348.
63. Beuche W, Yushchenko M, Mader M, Maliszewska M, Felgenhauer K, Weber F. Matrix metalloproteinase-9 is elevated in serum of patients with amyotrophic lateral sclerosis. *Neuroreport*. 2000;11(16):3419–3422.
64. Fang L, Huber-Abel F, Teuchert M, et al. Linking neuron and skin: Matrix metalloproteinases in amyotrophic lateral sclerosis (ALS). *J Neurol Sci*. 2009;285(1-2):62–66.
65. Bell RD, Winkler EA, Singh I, et al. Apolipoprotein E controls cerebrovascular integrity via cyclophilin A. *Nature*. 2012; 485(7399):512–516.
66. Solomon DA, Mitchell JC, Salcher-Konrad M-T, Vance CA, Mizielinska S. Review: Modelling the pathology and behaviour of frontotemporal dementia. *Neuropathol Appl Neurobiol*. 2019;45(1):58–80.
67. Berning BA, Walker AK. The pathobiology of TDP-43 C-terminal fragments in ALS and FTLD. *Front Neurosci*. 2019;13:335.
68. Le Ber I, Guedj E, Gabelle A, et al. Demographic, neurological and behavioural characteristics and brain perfusion SPECT in frontal variant of frontotemporal dementia. *Brain J Neurol*. 2006; 129(11):3051–3065.
69. Bersano E, Sarnelli MF, Solara V, et al. Decline of cognitive and behavioral functions in amyotrophic lateral sclerosis: A longitudinal study. *Amyotroph Lateral Scler Front Degener*. 2020;21(5-6): 373–379.
70. Burrell JR, Kiernan MC, Vucic S, Hodges JR. Motor neuron dysfunction in frontotemporal dementia. *Brain*. 2011;134(Pt 9): 2582–2594.
71. Lulé DE, Aho-Özhan HEA, Vázquez C, et al. Story of the ALS-FTD continuum retold: Rather two distinct entities. *J Neurol Neurosurg Psychiatry*. 2019;90(5):586–589.
72. Baker M, Mackenzie IR, Pickering-Brown SM, et al. Mutations in progranulin cause tau-negative frontotemporal dementia linked to chromosome 17. *Nature*. 2006;442(7105):916–919.
73. Ghezzi P, Casagrande S, Massignan T, et al. Redox regulation of cyclophilin A by glutathionylation. *Proteomics*. 2006;6(3): 817–825.
74. Lammers M, Neumann H, Chin JW, James LC. Acetylation regulates cyclophilin A catalysis, immunosuppression and HIV isomerization. *Nat Chem Biol*. 2010;6(5):331–337.